

# Enrichment of the Galactic disc with neutron capture elements: Sr <sup>\*</sup> †

T. Mishenina<sup>1</sup>, M. Pignatari<sup>2,3,4</sup>, T. Gorbaneva<sup>1</sup>, S. Bisterzo<sup>5,6,4</sup>, C. Travaglio<sup>5,6,4</sup>, F.-K. Thielemann<sup>7</sup>, C. Soubiran<sup>8</sup>

<sup>1</sup> *Astronomical Observatory, Odessa National University, and*

*Isaac Newton Institute of Chile, Odessa branch, Shevchenko Park, 65014, Odessa, Ukraine*

<sup>2</sup> *E.A. Milne Centre for Astrophysics, Dept of Physics & Mathematics, University of Hull, HU6 7RX, United Kingdom*

<sup>3</sup> *Konkoly Thege Miklos ut 15-17, H-1121 Budapest, Hungary*

<sup>4</sup> *The NuGrid collaboration, <http://www.nugridstars.org>*

<sup>5</sup> *INFN, Istituto Nazionale Fisica Nucleare, Via Pietro Giuria, 1, 10125, Turin, Italy*

<sup>6</sup> *B2FH Association, Turin, Italy*

<sup>7</sup> *Department of Physics, University of Basel, Klingelbergstrabe 82, 4056 Basel, Switzerland*

<sup>8</sup> *Laboratoire d'Astrophysique de Bordeaux, Univ. Bordeaux - CNRS, B18N, allée Geoffroy Saint-Hilaire, 33615 Pessac, France*

Accepted 2015 xxx. Received 2015 xxx; in original form 2015 xxx

## ABSTRACT

The enrichment history of heavy neutron-capture elements in the Milky Way disc provides fundamental information about the chemical evolution of our Galaxy and about the stellar sources that made those elements. In this work we give new observational data for Sr, the element at the first neutron-shell closure beyond iron,  $N=50$ , based on the analysis of the high resolution spectra of 276 Galactic disc stars. The Sr abundance was derived by comparing the observed and synthetic spectra in the region of the Sr I 4607 Å line, making use of the LTE approximation. NLTE corrections lead to an increase of the abundance estimates obtained under LTE, but for these lines they are minor near solar metallicity. The average correction that we find is 0.151 dex. The star that is mostly affected is HD 6582, with a 0.244 dex correction. The behavior of the Sr abundance as a function of metallicity is discussed within a stellar nucleosynthesis context, in comparison with the abundance of the heavy neutron-capture elements Ba ( $Z=56$ ) and Eu ( $Z=63$ ). The comparison of the observational data with the current GCE models confirm that the  $s$ -process contributions from Asymptotic Giant Branch stars and from massive stars are the main sources of Sr in the Galactic disc and in the Sun, while different nucleosynthesis sources can explain the high [Sr/Ba] and [Sr/Eu] ratios observed in the early Galaxy.

**Key words:** stars: abundances – stars: late-type – Galaxy: disc – Galaxy: evolution

## 1 INTRODUCTION

The study of the chemical enrichment history of stars in our Galaxy allows to benchmark our understanding in its formation and evolution, and in stellar evolution and nucleosynthesis. Across the evolution of the Galaxy elements have been made by different generations of stars, building up the abundance pattern observed today also in the Sun (e.g., Matteucci & Greggio 1986; Timmes, Woosley & Weaver 1995; Goswami & Prantzos 2000; Gibson et al. 2003; Kobayashi, Karakas & Umeda

2011). Despite their low abundance relative to other metals lighter than iron, heavy elements provide powerful constraints for chemical evolution and other nuclear astrophysics disciplines. According to the established scenario of nucleosynthesis of heavy elements in stars, about half of the abundances beyond iron are due to the slow neutron capture process or  $s$ -process (e.g., Käppeler et al. 2011, and references therein), and half to the rapid neutron capture process, or  $r$ -process (e.g., Thielemann et al. 2017; Cowan et al. 2019, and references therein). However, in the last twenty years a growing amount of theoretical and observational works provide the evidence of the existence of other nucleosynthesis processes feeding the production of heavy elements, at least up to the first neutron-magic

\* Based on observations collected at OHP observatory, France

† Table A1 is only available in electronic form

peak beyond Fe, where elements Sr, Y and Zr are located. Different types of neutrino-driven wind components from forming proto-neutron stars in Core-Collapse Supernovae (CCSNe) have been shown to potentially contribute to the production of these elements, at least in the early Galaxy (e.g., Fröhlich et al. 2006; Farouqi et al. 2009; Arcones & Montes 2011; Roberts, Woosley & Hoffman 2010; Wanajo, Janka & Kubono 2011; Martínez-Pinedo, Fischer & Huther 2014; Curtis et al. 2019). Wanajo, Janka & Müller (2011) discussed as well the nucleosynthesis production of these elements in electron-capture supernovae.

A number of nucleosynthesis processes needed at low metallicity have been also discussed by Hansen, Montes & Arcones (2014), utilizing the approach by Qian & Wasserburg (2001). These authors considered neutrino-driven winds in CCSNe as a source of Sr. More recent analyses of production of elements at the Sr peak in metal-poor stars are provided by Hansen et al. (2018) and Spite et al. (2018).

In this context, a clear understanding of the production of elements in the Sr-Y-Zr region becomes more complicated compared to the established two-components scenario, where only the *s*-process and the *r*-process are relevant. Many processes need to be taken into account to explain the observed abundances, and their relative relevance may change across the history of the Galaxy. In the Galactic halo the role of *s*-process production from Asymptotic Giant Branch (AGB) stars in Galactic Chemical Evolution (GCE) is minor, even for elements that are typically classified as *s*-process elements by looking at the abundance distribution in the solar system (e.g., Travaglio et al. 2004). Recent GCE simulations by Bisterzo et al. (2014) assign to Sr an *s*-process contribution from AGB stars of  $68.9 \pm 5.9$  %, but that contribution is not significant for Sr observed in metal-poor stars. On the other hand, *s*-process in fast rotating metal poor stars could provide a significant contribution to Sr production observed in Galactic halo stars (Pignatari et al. 2008; Frischknecht et al. 2016), and could be marginal for the Sr abundance in the Galactic disc. A study of the Sr/Ba ratio in four halo stars (Spite et al. 2014) has shown that the abundance pattern of the *s*-process elements is strikingly similar to the theoretical estimates of the *s*-process. The contribution to the *s*-process by rapidly rotating stars (Meynet & Maeder 2017; Choplin et al. 2017; Nishimura et al. 2017) as the missing component responsible for the relative distribution of the light (Sr) and heavy (Ba) neutron-capture elements has been studied by adopting a stochastic chemical evolution model (Cescutti et al. 2015b).

Travaglio et al. (2004) found that in the solar abundances there is a component missing between Sr and Xe, not explained by the traditional *s*-process and *r*-process scenario. They called that component Lighter Element Primary Process or LEPP, and associated to the Sr-rich signature observed in a large fraction of metal-poor stars. This result is still controversial (see e.g., Honda et al. 2004, 2007; Montes et al. 2007; Trippella et al. 2016; Cristallo et al. 2015). Travaglio et al. results were not taking into account all the zoo of processes possibly feeding at least the Sr-Y-Zr peak, and it is plausible that some of them will be relevant for GCE. Sr is made from the weak *s*-process in massive stars (e.g., Raiteri et al.

1991a,b; Pignatari et al. 2010; The, El Eid & Meyer 2007; Pignatari et al. 2016b) and in massive AGB stars ( $> 4 M_{\odot}$ ) (e.g., Karakas & Lattanzio 2014; Cristallo et al. 2015; Pignatari et al. 2016a). Travaglio et al. (2004) estimated the contribution by the weak *s*-process to be 9% of the solar Sr. The contribution from massive AGB stars changes between 9% (Travaglio et al. 2004) to 1.35% by (Bisterzo et al. 2014). There is not a clear estimate of the errors associated to these contributions, where both nuclear and stellar model uncertainties are consistently taken into account (e.g., Pignatari et al. 2016a). The *r*-process, together with all of these nucleosynthesis processes, made the remaining part of Sr that was not created by the *s*-process. However, also the origin of the *r*-process elements with  $A > 56$  remains controversial. At least four sources have been proposed, namely: 1) the neutrino-induced winds from supernovae (Woosley et al. 1994; Takahashi, Witt & Janka 1994); 2) the neutron-rich matter ejected from coalescing neutron stars (Freiburghaus, Rosswog & Thielemann 1999; Thielemann et al. 2017) (see further references in the latter review); 3) the winds from the black hole-neutron stars mergers (Surman et al. 2008); and 4) polar jet ejecta from magneto-rotational supernovae (Winteler et al. 2012; Nishimura, Takiwaki & Thielemann 2015; Nishimura et al. 2017).

In the last years the intermediate-neutron capture process or *i*-process (Cowan & Rose 1977) has been shown to be active since the first stages of the evolution of the Galaxy, possibly explaining anomalous abundance patterns observed in old metal-poor stars (e.g., Dardelet et al. 2014; Hampel et al. 2016; Roederer et al. 2016; Clarkson, Herwig & Pignatari 2018), in younger objects in the Galactic disc and in open clusters (Herwig et al. 2011; Mishenina et al. 2015; D’Orazi, De Silva & Melo 2017) and in presolar grains (Fujiya et al. 2013; Liu et al. 2014).

Also alternative sources have been introduced in several papers (Travaglio et al. 2004; Qian & Wasserburg 2008). For example, the role of neutron star mergers in the chemical evolution of the Galactic halo and the *r*-process production of Sr, Zr, and Ba - complemented by an *s*-process production from spinstars was presented in Cescutti et al. (2015a). Both neutron star mergers and supernova scenarios might have contribute in producing Eu, and observations at low metallicity allow to identify two components of *r*-process nucleosynthesis (e.g., Wehmeyer, Pignatari & Thielemann 2015). Indeed, theoretical *r*-process estimates can be tested directly with Galactic Archaeology, by looking at the composition of stars formed with insufficiently mixed matter, and enriched with heavy elements resulting from one or few early *r*-process events (e.g. Aoki et al. 2007; Sneden, Cowan & Gallino 2008; Roederer et al. 2010).

The Sr abundance was studied in 156 stars of the Galactic disc in a recent paper by Battistini & Bensby (2016). The authors concluded that the *s*-process is responsible for the main contribution in the enrichment of Sr, with an additional contribution from a non-classical *r*-process at low metallicities. In the thin disc the trends of  $[El/Fe]$  vs.  $[Fe/H]$  are flatter, which is due to the fact that the main production from the *s*-process is balanced by Fe production from type Ia supernovae. With metallicities in the range from  $-1 < [Fe/H] < 0.3$  dex the contributions to neutron capture elements by

all mentioned processes are different, and they change in the course of the Galaxy evolution. In previous studies we have determined the abundances of a number of neutron-capture elements for more than 250 stars (Mishenina et al. 2013). Here we extend our study with information on Sr, and we provide a comparative analysis of the abundances of elements that in the Galactic disc are mostly made by the  $s$ -process (Sr and Y at the neutron shell closure  $N=50$ , and Ba and La at  $N=82$ )  $s$ -process elements in relation to europium (Eu), produced by  $r$ -process.

The paper is organized as follow. The observations and selection of stars plus the definition of the main stellar parameters are described in §2. The abundance determinations and the error analysis are presented in §3. The results and comparison with other data as well as the application of the results to the theory of nucleosynthesis and the chemical evolution of the Galaxy are reported in §4. Conclusions are drawn in §5.

## 2 OBSERVATIONS AND ATMOSPHERIC PARAMETERS

Most observations used here were previously analysed in our paper on  $n$ -capture elements (Mishenina et al. 2013). The spectra were obtained using the 1.93 m telescope at Observatoire de Haute-Provence (OHP, France) equipped with the echelle type spectrographs ELODIE ( $R = 42000$ ) for the wavelengths range 4400 – 6800 Å and signal to noise S/N more than 100. Our starting sample includes 276 stars like in Mishenina et al. (2013). Also for those stars we have searched additional spectra in the OHP spectroscopic archive (Moultaka et al. 2004), from the SOPHIE spectrograph which cover a similar wavelength range at a resolution of  $R= 75000$ . The primary processing of spectra was carried out immediately during observations (Katz et al. 1998). Further spectra processing such as the continuum placement, line depth and equivalent width (EW) measurements, etc., was conducted using the DECH20 software package by Galazutdinov G. A. (1992).

This paper belongs to a set of studies of abundances in stars in the galactic disc (Mishenina et al. 2004, 2008, 2013). We use the same stellar parameters derived for stars in our sample. To estimate the effective temperatures  $T_{\text{eff}}$ , we used one and the same approach for 267 dwarfs in our sample; in so doing, for better control we have applied the far-wing fitting of the  $H_{\alpha}$  line profiles for nine stars with metallicities below  $-0.6$  dex, and that turned out to be more suitable. Since the far-wings of  $H_{\alpha}$  are independent from gravity, metallicity and convection of the atmosphere model (Gratton, Carretta & Castelli 1996), and also to avoid uncertainties in the calibrations which were constructed in the range of  $-0.5 < [\text{Fe}/\text{H}] < +0.5$  and used by us for a large part of dwarfs. Effective temperatures  $T_{\text{eff}}$  were determined by the calibration of line-depth ratios for spectral line pairs with significantly different low-level excitation potential applying the technique introduced and developed by Kovtyukh et al. (2003). The mean random error of each single calibration was 60-70 K (it ranged from 40-45 K to 90-95 K for the most and least accurate calibrations, respectively). The usage of about 70 - 100 calibrations enabled us to reduce the uncertainty down to 5-7 K (for

the spectra with S/N ratio of 100-150). It has been shown that 105 calibrations are essentially independent of microturbulence, departures from LTE (Local Thermodynamic Equilibrium), elemental abundances, rotational parameters or any other individual stellar properties. The estimated accuracy of the method varied within the range from 5 to 45 K for the dwarfs with  $[\text{Fe}/\text{H}] \geq -0.5$ . For most of metal-poor stars of the sample,  $T_{\text{eff}}$  was estimated by the far-wing fitting of the  $H_{\alpha}$  line profiles (Mishenina & Kovtyukh 2001). We have proved in Mishenina et al. (2004) that the temperature scales adopted in (Mishenina & Kovtyukh 2001) and (Kovtyukh et al. 2003) are well consistent.

Surface gravities  $\log g$  were computed by the ionization balance, implying that the iron abundances obtained from the neutral iron Fe I and ionized iron Fe II lines were similar. The two most-commonly used techniques for the surface gravity determination are the ionization balance of neutral and ionized species and the fundamental relation expressing the gravity as a function of the mass, temperature and bolometric absolute magnitude deduced from the parallax. A detailed study of surface gravities derived by different methods was performed by Allende Prieto et al. (1999), who reported that astrometric and spectroscopic (iron ionization balance) gravities were in good agreement within the metallicity range of  $-1.0 < [\text{Fe}/\text{H}] < +0.3$ . In our earlier paper (Mishenina et al. 2004), we compared the adapted surface gravities to those determined astrometrically by Allende Prieto et al. (1999); the resulting mean difference and standard deviation were  $-0.01$  and  $0.15$ , respectively, for 39 common stars. This is consistent with an accuracy of 0.1 dex of our spectroscopic gravity determinations. Moreover, in each of our studies, we have been analysing the correlation between our estimates of chemical abundances and stellar parameters to justify the correctness of the latter.

The adopted value of the metallicity  $[\text{Fe}/\text{H}]$  was calculated using the iron abundance obtained from the Fe I lines. As is known (e.g. Thévenin & Idiart 1999; Shchukina & Trujillo Bueno 2001; Mashonkina et al. 2011; Bergemann et al. 2012), the lines of neutral iron are influenced by the deviations from the LTE in solar and stellar spectra, and hence, these deviations also affect the iron abundances determined from those lines. However, within the temperature and metallicity ranges of our target stars, the NLTE corrections do not exceed 0.1 dex (see, e.g. Mashonkina et al. 2011).

The microturbulent velocity  $V_t$  was derived considering that the iron abundance obtained from a given Fe I line is not correlated with the equivalent width EW of that line.

The obtained parameter values and their comparison with the results of other authors are reported in Mishenina et al. (2004, 2008, 2013). The accuracy of our parameter determination is estimated to be:  $\Delta T_{\text{eff}} = \pm 100$  K,  $\Delta \log g = \pm 0.2$  dex,  $\Delta V_t = \pm 0.2$  km s $^{-1}$ ,  $\Delta [\text{Fe}/\text{H}] = \pm 0.1$  dex. In this study, we have compared the adopted parameters with those obtained recently by Battistini & Bensby (2016) and Delgado Mena et al. (2017) who reported the Sr abundances estimated in the LTE approximation using the same Sr I line as in this study. In particular, our goal was to assess the  $T_{\text{eff}}$  scale in our study, which is essential for the Sr abundance determinations. The results of the comparison for individual stars are given in Table 1 while Table 2

presents the mean differences and errors (standard deviations) in the parameter values for the common set of target stars in various papers. In these Tables, we have also provided the results of the comparison of our Sr data with those obtained earlier (Reddy et al. 2003; Mashonkina & Gehren 2001; Brewer & Carney 2006); note, the Sr II line was used in the last two studies.

We find the concordance between our data and those by Battistini & Bensby (2016) within the stated error definitions, except for  $T_{\text{eff}}$  for the stars HD 135204, 152391, 157089, 159482, 199960, 201891 and for  $\log g$  for the star HD 135204. At that the average difference values of  $\langle \Delta T_{\text{eff}} \rangle$ ,  $\langle \Delta \log g \rangle$ ,  $\langle \Delta [\text{Fe}/\text{H}] \rangle$  are equal to  $-4 \pm 116$ ,  $-0.13 \pm 0.15$ ,  $-0.03 \pm 0.07$ , respectively. Matching our results with those of Delgado Mena et al. (2017) we obtained the average values  $\langle \Delta T_{\text{eff}} \rangle = 27 \pm 36$ ,  $\langle \Delta \log g \rangle = -0.08 \pm 0.13$ ,  $\langle \Delta [\text{Fe}/\text{H}] \rangle = -0.01 \pm 0.03$ , which show a good agreement between themselves.

Earlier, we carried out the kinematic classification of the thin and thick disc stars, as well as of the Hercules stream stars (Mishenina et al. 2004), based on the Hipparcos (ESA 1997) parallaxes and proper motions combined with radial velocities measured by the cross-correlation of the ELODIE spectra (with an accuracy better than  $100 \text{ m s}^{-1}$ ). We have not updated our classification with respect to the latest astrometric data from the *Gaia* Data Release 2 (Gaia Collaboration et al. 2018) either due to the fact that many stars of our sample are too bright to be measured by *Gaia* or that the relevant astrometric errors are equivalent to those of the Hipparcos observations. The classification is based on the (U, V, W) velocities with respect to the Sun with typical errors of  $1 \text{ km s}^{-1}$ . Having assumed that our sample represents three populations of stars in the solar vicinity, such as those of the thin and thick disc, as well as the Hercules stream group, we have computed the probability of each star's membership in either of these populations. In these computations, we have adapted the velocity ellipsoids determined by Soubiran, Bienaymé & Siebert (2003). A star is considered to belong to a certain population if the probability was higher than 70%. Application of this criterion implies that there are a number of stars with intermediate kinematics which cannot be classified.

### 3 DETERMINATION OF SR ABUNDANCES

The determination of the Sr abundance was obtained with the new version of the STARS LTE spectral synthesis code (Tsymbal 1996) from the Sr I line  $4607 \text{ \AA}$  using the stellar models (Castelli & Kurucz 2004). A comparison of synthetic and observed spectra for the Sr line is shown in Fig. 1.

The Sr abundance was determined by differential analysis relative to solar one. Solar abundances were calculated using the solar profiles, measured in the spectra of the Moon and asteroids; they were also estimated using the SOPHIE spectrograph and the oscillator strengths  $\log gf$  adopted from the VALD database (Kupka F. et al. 1999). Our approved LTE solar Sr abundance is  $\log A(\text{Sr})_{\odot} = 2.74 \pm 0.03$  in comparison to  $2.87 \pm 0.07$  (Asplund et al. 2009),  $2.83 \pm 0.06$  (Grevesse et al. 2015), and  $2.78$  (Delgado Mena et al. 2017). It should be emphasized that in Battistini & Bensby (2016) the values of the solar Sr abundance determined from the

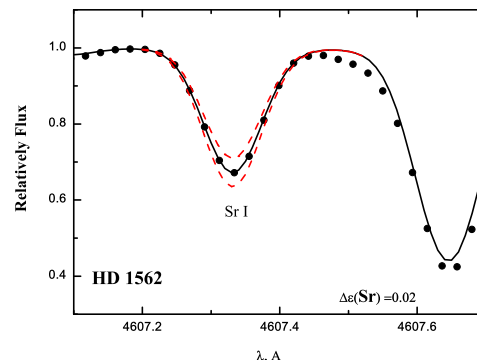


**Figure 1.** Observed (dots) and calculated (solid and dashed lines) spectra in the region of Sr I line for HD 1562, the change in the Sr abundance is 0.02 dex.

line  $4607 \text{ \AA}$  in the spectra of reflected sunlight obtained from different spectrographs with various resolutions are given. These values noticeably different (about 0.2 dex), ranging from  $\log A(\text{Sr})_{\odot}(\text{MIKE}) = 2.69$  to  $\log A(\text{Sr})_{\odot}(\text{FEROS}) = 2.92$ , where  $\log A(\text{H}) = 12.0$ . This is important to keep in mind and take into account when determining the content of elements relative to solar one, since it may generate a systematic shift of observational data. The departures from LTE and their effect on the determination of the Sr abundances for stars with different metallicities have been investigated in a number of papers (e.g. Belyakova & Mashonkina 1997; Mashonkina & Gehren 2001; Andrievsky et al. 2011), wherein the Sr II lines were analysed. An NLTE analysis of the Sr I and Sr II lines in the spectra of late-type stars was performed by Bergemann et al. (2012). The model of the Sr atom was constructed using the atomic data available in the Hannover and NIST databases. The neutral atom was represented by 141 levels; the singly-ionized atom included 49 levels. The described model of Sr was similar to that one created by Andrievsky et al. (2011) with regard to the term structure and the number of dipole-permitted transitions of Sr II, but unlike the latter it factored in the effect of deviations from LTE on the neutral Sr line (for more details see Bergemann et al. (2012)). A grid of the NLTE abundance corrections for Sr I and Sr II lines was presented in (Bergemann et al. 2012). The NLTE corrections for the Sr I line  $4607 \text{ \AA}$  reported in (Bergemann et al. 2012) for dwarfs varied within the range of  $0.10 - 0.23$  dex at  $[\text{Fe}/\text{H}] > -0.8$  dex, depending on the temperature and metallicity of star. Using the data of Bergemann et al. (2012), we have interpolated the values of the NLTE corrections for the Sr I line  $4607 \text{ \AA}$  for our target stars. The NLTE Sr correction for the Sun is 0.10 dex. For metal poor stars it is more suitable to use the Sr II lines which have smaller NLTE corrections, not exceeding 0.2 dex (Andrievsky et al. 2011) or close to 0.05 dex (Hansen et al. 2013).

The obtained LTE Sr abundances, the NLTE corrections from Bergemann et al. (2012), the NLTE Ba and LTE Eu abundance, and stellar parameters (Mishenina et al. 2013) are given in Table A1 which is available on-line.

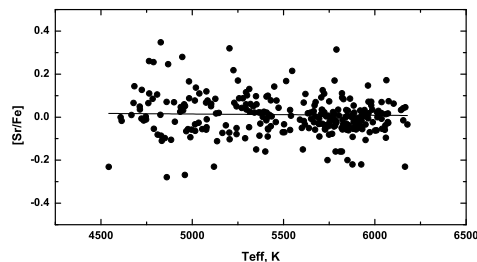
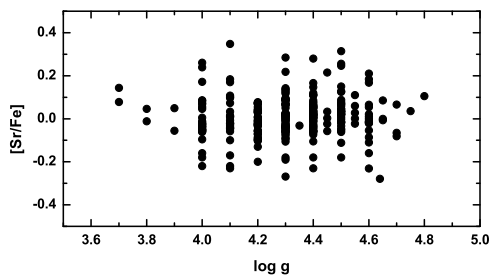
Fig. 4 presents our observations and a comparison with GCE predictions by Bisterzo et al. (2014) and

**Table 1.** Parameters of our target stars and comparison with Battistini & Bensby (2016); Delgado Mena et al. (2017); Mashonkina & Gehren (2001); Reddy et al. (2003); Brewer & Carney (2006) for common stars.

HD	$T_{\text{eff}}$ , K	$\log g$	[Fe/H]	HD	$T_{\text{eff}}$ , K	$\log g$	[Fe/H]	$\Delta T_{\text{eff}}$ , K	$\Delta \log g$	$\Delta$ [Fe/H]
our				Battistini & Bensby (2016)						
8648	5841	4.3	0.22	8648	5790	4.2	0.12	51	0.1	0.1
22879	5972	4.5	-0.77	22879	5825	4.42	-0.91	145	0.08	0.1
30495	5790	4.5	0.02	30495	5820	4.4	-0.05	-30	0.1	0.07
64606	5188	4.4	-0.91	64606	5250	4.2	-0.91	-62	0.2	0
64815	5763	3.9	-0.35	64815	5864	4	-0.33	-101	-0.1	-0.02
135204	5200	4.4	-0.19	135204	5413	4	-0.16	-213	0.4	-0.03
152391	5322	4.5	-0.08	152391	5495	4.3	-0.08	-173	0.2	0
157089	5915	4.3	-0.5	157089	5785	4	-0.56	130	0.3	-0.06
159482	5760	4.3	-0.81	159482	5620	4.1	-0.89	140	0.2	0.08
159909	5671	4.3	0.03	159909	5749	4.1	0.06	-78	0.2	-0.03
165401	5794	4.5	-0.4	165401	5877	4.3	-0.36	-83	0.2	-0.04
178428	5656	4.2	0.15	178428	5695	4.4	0.14	-39	-0.2	0.01
187897	5944	4.5	0.12	187897	5887	4.3	0.08	57	0.2	0.04
190360	5572	4.5	0.26	190360	5606	4.4	0.12	-34	0.1	0.14
199960	6023	4.4	0.33	199960	5878	4.2	0.23	145	0.2	0.1
201891	5973	4.3	-1.08	201891	5850	4.4	-0.96	123	-0.1	-0.12
217014	5858	4.4	0.24	217014	5763	4.3	0.17	95	0.1	0.07
our				Delgado Mena et al. (2017)						
4307	5889	4.0	-0.18	4307	5840	4.13	-0.21	49	-0.13	0.03
14374	5449	4.3	-0.09	14374	5375	4.42	-0.07	74	-0.12	-0.03
22049	5084	4.4	-0.15	22049	5049	4.45	-0.15	35	-0.05	0.0
22879	5972	4.5	-0.77	22879	5949	4.68	-0.79	23	-0.18	0.02
38858	5776	4.3	-0.23	38858	5719	4.49	-0.23	57	-0.19	0.00
76151	5776	4.4	0.05	76151	5781	4.44	0.12	-5	-0.04	-0.07
125184	5695	4.3	0.31	125184	5660	4.11	0.27	35	0.19	0.04
146233	5799	4.4	0.01	146233	5810	4.46	0.05	-11	-0.06	-0.04
161098	5617	4.3	-0.27	161098	5574	4.49	-0.26	43	-0.19	-0.01
199960	5878	4.2	0.23	199960	5928	4.42	0.27	-50	-0.22	-0.04
210752	6014	4.6	-0.53	210752	5970	4.52	-0.55	44	0.08	0.02
our				Mashonkina & Gehren (2001)						
4614	5965	4.4	-0.24	4614	5940	4.33	-0.3	25	0.07	0.06
22879	5972	4.5	-0.77	22879	5870	4.27	-0.86	102	0.23	0.09
55575	5949	4.3	-0.31	55575	5890	4.25	-0.36	59	0.05	0.05
64606	5250	4.2	-0.91	64606	5320	4.54	-0.89	-70	-0.34	-0.02
65583	5373	4.6	-0.67	65583	5320	4.55	-0.73	53	0.05	0.06
68017	5651	4.2	-0.42	68017	5630	4.45	-0.40	21	-0.25	-0.02
109358	5897	4.2	-0.18	109358	5860	4.36	-0.21	37	-0.16	0.03
112758	5203	4.2	-0.56	112758	5240	4.62	-0.43	-37	-0.42	-0.13
114710	5954	4.3	0.07	114710	6000	4.30	-0.03	-46	0.0	0.1
117176	5611	4.0	-0.03	117176	5480	3.83	-0.11	131	0.17	0.08
126053	5728	4.2	-0.32	126053	5690	4.45	-0.35	38	-0.25	0.03
144579	5294	4.1	-0.70	144579	5330	4.59	-0.69	-36	-0.49	-0.01
168009	5826	4.1	-0.01	168009	5785	4.23	-0.03	41	-0.13	0.02
176377	5901	4.4	-0.17	176377	5860	4.43	-0.27	41	-0.03	0.1
our				Reddy et al. (2003)						
11007	5980	4	-0.2	11007	5850	4	-0.31	130	0	0.11
42618	5787	4.5	-0.07	42618	5653	4.58	-0.16	134	-0.08	0.09
45067	6058	4	-0.02	45067	5946	3.99	-0.12	112	0.01	0.1
71148	5850	4.2	0	71148	5703	4.46	-0.08	147	-0.26	0.08
126053	5728	4.2	-0.32	126053	5597	4.44	-0.41	131	-0.24	0.09
186408	5803	4.2	0.09	186408	5670	4.32	0	133	-0.12	0.09
206860	5927	4.6	-0.07	206860	5820	4.48	-0.12	107	0.12	0.05
our				Brewer & Carney (2006)						
25665	4967	4.7	0.01	25665	4870	4.4	-0.012	97	0.3	0.022
53927	4860	4.64	-0.22	53927	4960	4.6	-0.385	-100	0.04	0.165
159062	5414	4.3	-0.4	159062	5260	4.45	-0.507	154	-0.15	0.107
168009	5826	4.1	-0.01	168009	5720	4.2	-0.07	106	-0.1	0.06

**Table 2.** Comparison of our parameters and Sr abundance determinations with the results of other authors for the  $n$  stars shared with our stellar sample.

Reference	$\Delta(T_{\text{eff}})$	$\Delta(\log g)$	$\Delta([\text{Fe}/\text{H}])$	$\Delta([\text{Sr}/\text{Fe}])$	$n$
Battistini & Bensby 2016	4 $\pm 116$	0.13 $\pm 0.15$	0.03 $\pm 0.07$	-0.01 -	17 (1)
Delgado Mena et al. 2017	27 $\pm 36$	-0.08 $\pm 0.13$	-0.01 $\pm 0.03$	-0.05 $\pm 0.09$	12
Mashonkina & Gehren 2001	26 $\pm 56$	-0.10 $\pm 0.21$	0.03 $\pm 0.06$	0.02 $\pm 0.10$	14
Reddy et al. 2003	127 $\pm 13$	-0.08 $\pm 0.14$	0.09 $\pm 0.02$	-0.03 $\pm 0.08$	7
Brewer & Carney 2006	64 $\pm 112$	0.02 $\pm 0.20$	0.09 $\pm 0.06$	-0.21 $\pm 0.22$	4

**Figure 2.** Dependence of  $[\text{Sr}/\text{Fe}]$  vs.  $T_{\text{eff}}$ .**Figure 3.** Dependence of  $[\text{Sr}/\text{Fe}]$  vs.  $\log g$ .

### 3.1 Errors in abundance determinations

To determine the systematic errors in the elemental abundances, resulting from uncertainties in the atmospheric parameters, we derived the elemental abundance of two stars HD216259 ( $T_{\text{eff}} = 4833$  K,  $\log g = 4.60$ ,  $V_t = 0.5$  km/s,  $[\text{Fe}/\text{H}] = -0.55$ ) and HD9826 ( $T_{\text{eff}} = 6074$  K,  $\log g = 4.00$ ,  $V_t = 1.3$  km/s,  $[\text{Fe}/\text{H}] = 0.10$ ) for several models with modified parameters ( $\Delta T_{\text{eff}} = \pm 100$  K,  $\Delta \log g = \pm 0.2$ ,  $\Delta V_t = \pm 0.1$ ). The abundance variations with the modified parameters and the fitting errors for the computed and observed spectral line profiles (0.02 dex), are given in Table 3. The maximum contribution to the error is introduced by  $T_{\text{eff}}$ . Total errors due to parameter uncertainties and the measured spectra varies from 0.12 dex for the hot and to 0.06 – 0.17 dex for the cool stars. The dependence of the Sr abundance on stellar parameters ( $T_{\text{eff}}$  and  $\log g$ ) is presented in Figs. 2 and 3. No trend of  $[\text{Sr}/\text{Fe}]$  vs.  $T_{\text{eff}}$  and  $\log g$  is observed.

We compare our LTE Sr abundances with the ones obtained by Battistini & Bensby (2016) in LTE assumption who used the same Sr I line 4607 Å as in our case. We have only one star in common (HD 64606) with that work, for which Sr abundance is provided. The difference in the Sr abundance of HD 64606 is consistent within 0.01 dex. The mean values of the difference between our LTE definitions and those of (Delgado Mena et al. 2017) is equal to  $-0.05 \pm 0.09$ , confirming the overall agreement with our determinations. For five stars (HD 22049, HD 22879, HD 38858, HD 125184, HD 161098) the individual differences are larger than 0.05 dex, as highlighted in Fig. 5. As can be seen from the figures, a significant scatter in  $[\text{Sr}/\text{Fe}]$  ratio is observed. In our stellar sample, we obtain an observed range  $-0.28 \lesssim [\text{Sr}/\text{Fe}] \lesssim 0.34$  for thin disc stars, which is higher than what the range measured for more metal-poor thin-disc stars (from  $-0.03 \lesssim [\text{Sr}/\text{Fe}] \lesssim 0.26$  dex). This is likely due to a smaller sample of metal-poor stars, providing a less meaningful comparison. We have good agreement with results by Delgado Mena et al. (2017) for thin-disc stars with solar-like metallicity ( $-0.19 \lesssim [\text{Sr}/\text{Fe}] \lesssim 0.29$  dex), while they obtain a larger scatter for Sr abundances in metal-poor stars ( $-0.36 \lesssim [\text{Sr}/\text{Fe}] \lesssim 0.40$  dex). Greater variation of Sr abundances is shown by Battistini & Bensby (2016) ( $-0.37 \lesssim [\text{Sr}/\text{Fe}] \lesssim 0.54$  dex). Their results are obtained in the LTE approximation, but the NLTE corrections are positive, meaning that NLTE corrections will not improve the situation for moderately metal-poor stars. Taking into ac-

Travaglio et al. (2004), and also the interpolated NLTE corrections from Bergemann et al. (2012). Fig. 5 shows a comparison between our data and those of Battistini & Bensby (2016) and Delgado Mena et al. (2017), with GCE model by Bisterzo et al. (2014).

**Table 3.** Abundance errors due to atmospheric parameter uncertainties as examples of stars with different values of stellar parameters: HD216259 (4833,4.60,0.5,-0.55) and HD9826 (6074,4.00,1.3,0.10).

		HD216259			HD9826				
AN	El	$\Delta T_{\text{eff}}$	$\Delta \log g$	$\Delta Vt$	tot	$\Delta T_{\text{eff}}$	$\Delta \log g$	$\Delta Vt$	tot
38	SrI	0.15	-0.07	-0.04	0.17	0.12	0.00	-0.02	0.12

count observational data for  $[\text{Sr}/\text{Fe}]$  and their uncertainties, the observed dispersion of  $[\text{Sr}/\text{Fe}]$  is larger than the provided errors:  $\pm 0.15$  dex for our determinations, consistently with Battistini & Bensby (2016), and from 0.01 to 0.46 dex for the stellar data by Delgado Mena et al. (2017). Concerning the  $[\text{Sr}/\text{Fe}]$  trend with respect to  $[\text{Fe}/\text{H}]$ , based on our data for thin and thick discs we did not find any significant trend (slope  $-0.00379 \pm 0.02427$ ). Battistini & Bensby (2016) reported instead a mild increasing  $[\text{Sr}/\text{Fe}]$  abundance ratios with decreasing metallicity:  $[\text{Sr}/\text{Fe}] \approx -0.2$  for solar metallicity stars, increasing to  $[\text{Sr}/\text{Fe}] \approx 0$  at  $[\text{Fe}/\text{H}] \approx -1$ . Taking into account the large  $[\text{Sr}/\text{Fe}]$  scatter observed in the metal-poor stars, giants and dwarfs (e.g. Burris et al. 2000; Brewer & Carney 2006), over a metallicity range  $-2.0 < [\text{Fe}/\text{H}] < 0.2$ , the trend seems to be on average solar (e.g., Brewer & Carney 2006). Ishigaki, Aoki & Chiba (2013) observed thick disc and halo stars, also founding solar  $[\text{Sr}/\text{Fe}]$  ratios for  $[\text{Fe}/\text{H}] < -1$ . While there may be contradictory results concerning the observational trend of  $[\text{Sr}/\text{Fe}]$ , especially for metal-poor stars in the thick disc and in the halo, a significant real  $[\text{Sr}/\text{Fe}]$  dispersion beyond the observational error is a consistent result obtained from all authors.

As shown in the works (e.g. Belyakova & Mashonkina 1997; Mashonkina & Gehren 2001; Andrievsky et al. 2011; Bergemann et al. 2012) the NLTE corrections for the lines of neutral and ionized strontium depend on the stellar parameters ( $T_{\text{eff}}$ ,  $\log g$ , and  $[\text{Fe}/\text{H}]$ ). And, specifically, the dependence on metallicity affects the estimates of the strontium abundance in various Galactic substructures, primarily the halo and the disc, which differ in this parameter. For stars of lowest metallicity (halo), the Sr II line usually used to determine the strontium abundance, for which NLTE corrections are small (e.g. Andrievsky et al. 2011). The use of the Sr I lines requires the NLTE corrections from 0.05 to 0.5 (e.g. Bergemann et al. 2012), depending on the metallicity. As we show in Fig. 4, in our considered metallicity range, the average value of NLTE corrections is 0.151 dex, for stars of the thin disc, and for stars of the thick disc they change from 0.137 to 0.244 dex and there is the dependence on metallicity. The considering of the Sr abundance behaviour in the thin and thick disc stars has shown that the NLTE deviations change more the trend for the thick disc stars than for the thin disc stars. However, the scatter of the Sr abundance on all metallicity of the disc (and the Galaxy) does not allow a fine comparison of the Sr abundance in various substructures of the disc with predictions of models of Galactic evolution.

## 4 RESULTS AND COMPARISON WITH GCE MODELS

Element abundances measured in stars are an ideal yardstick for nucleosynthesis predictions and their effect on stellar and galactic evolution. The solar system abundance of the element Sr is dominated by the *s*-process contribution to  $^{88}\text{Sr}$  (82.6% of the solar Sr) by AGB stars.  $^{86}\text{Sr}$  and  $^{87}\text{Sr}$  (9.9% and 7.0% of the solar Sr, respectively) are *s*-only isotopes (Käppeler et al. 2011). Finally, the rarest Sr isotope is  $^{84}\text{Sr}$  (0.56% of the solar Sr), that is a product of *p*-process in stars (e.g., Rauscher et al. 2013; Pignatari et al. 2016a; Travaglio et al. 2018, and references therein).

As discussed in the introduction, a zoo of different nucleosynthesis processes can contribute to the production of Sr stable isotopes. Since spectroscopic observations can only determine element abundances for Sr, there exists no constraints on the isotopic pattern, excepting for the Sun. Therefore, it becomes difficult to disentangle the contribution from these different processes in stars in Galactic Archaeology studies (e.g., Yong et al. 2013), where few or even only one single nucleosynthesis event could dominate the isotopic abundance pattern. Sr is often used as a tracer of the LEPP enrichment in metal-poor stars (e.g., Montes et al. 2007). However, Sr elemental observations may lead to different interpretations. Fröhlich et al. (2006) suggested the  $\nu$ p-process as source of nuclei up to  $A=90$  or slightly beyond, originated in the neutrino-driven winds from forming neutron stars in CCSNe (see also more recent investigations by Martínez-Pinedo, Fischer & Huther 2014; Eichler et al. 2017). Due to the electron fraction  $Y_e$  larger than 0.5, the  $\nu$ p-process acts on the proton-rich side of the valley of stability, producing a non-solar isotopic pattern. The weak *s*-process, activated by the  $^{22}\text{Ne}$  neutron source in massive stars, is usually metallicity-dependent and negligible at low metallicities. However, in fast-rotating massive stars  $^{14}\text{N}$  can be made by rotational mixing, leading to a primary production of  $^{22}\text{Ne}$  in He-burning. The *s*-process production in fast-rotating massive stars has been investigated (Pignatari et al. 2008; Frischknecht et al. 2016; Meynet & Maeder 2017; Choplin et al. 2017; Nishimura et al. 2017; Prantzos et al. 2018), and considered by GCE modeling (Cescutti et al. 2015a; Bisterzo et al. 2017; Prantzos et al. 2018). On the other hand, as mentioned in the introduction the existence of the LEPP component is controversial (Cristallo et al. 2015; Trippella et al. 2016; Prantzos et al. 2018). A consistent set of observations over a large sample of stars such as the one presented in this work becomes instrumental to shed more light into this debate.

Our results for the Sr abundance obtained within the LTE approximation and the NLTE corrections (Bergemann et al. 2012) for our Sr determinations are shown in Fig. 4, in comparison to GCE model results

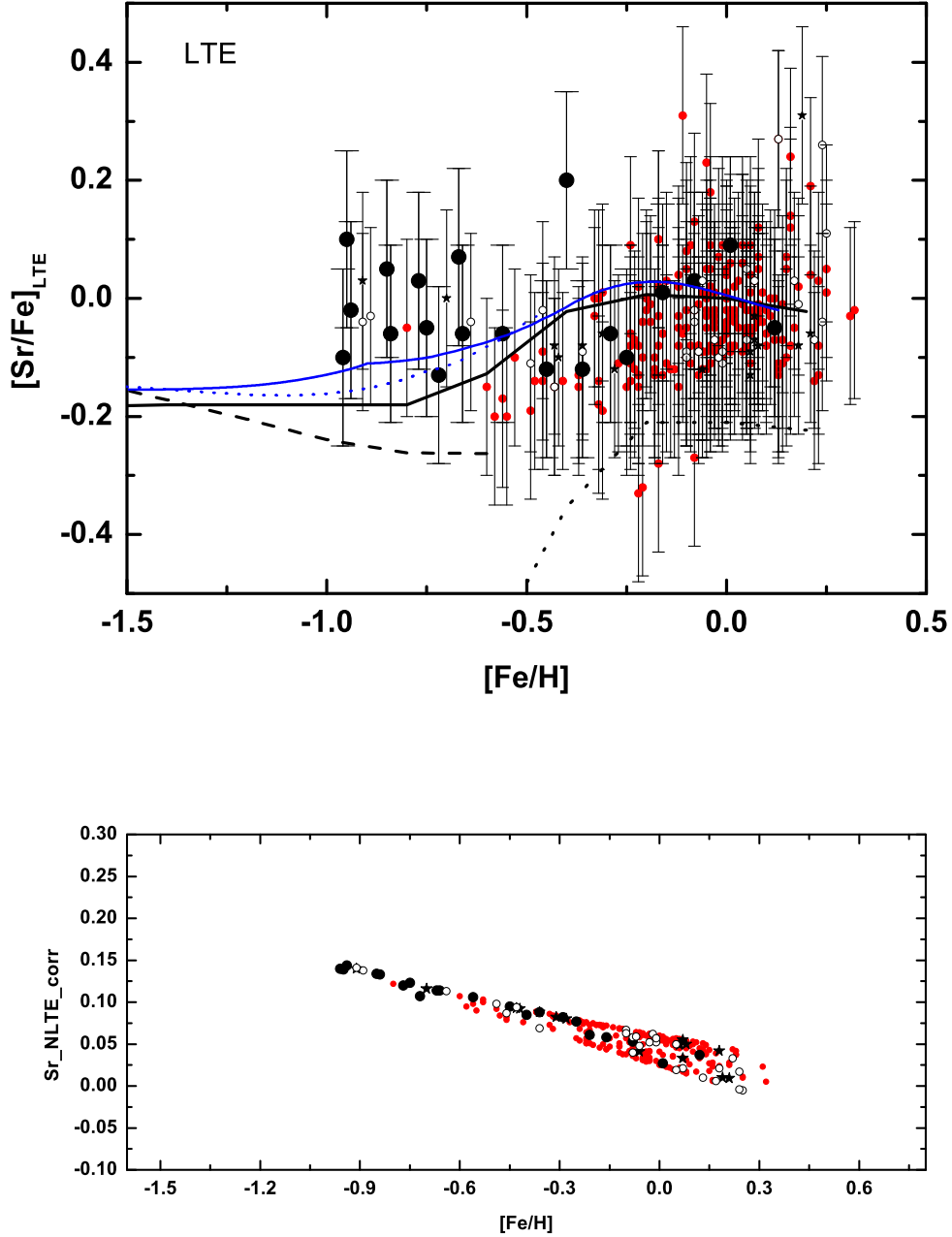


**Figure 4.** Our determination LTE (upper panel) Sr abundances (thin disc - red circles, thick disc - black circles, Hercules stream - asterisks, unclassified - open circles) and a comparison with models of Bisterzo et al. (2014) (thin disc - blue line, thick disc - dotted blue line) and Travaglio et al. (2004) (thin disc - black line, thick - black dashed line, only  $s$ -process contribution - black dotted line). NLTE corrections are from Bergemann et al. (2012) (bottom panel).



from Travaglio et al. (2004); Bisterzo et al. (2017). This GCE model (Travaglio et al. 2004) follows the composition of stars, stellar remnants, interstellar matter (atomic and molecular gas), and their mutual interaction, in the three main zones of the Galaxy, halo, thick disc, and thin disc. The chemical enrichment takes into account the  $s$ -process yields from AGB stars, the  $r$  contribution from massive stars (estimated with the residual method  $N_r = N_\odot - N_s$ ), and the primary LEPP contribution. As discussed in (Travaglio et al. 2004), the impact of AGB uncertainties on GCE computations may be partially reduced by assuming a range of  $^{13}\text{C}$ -pocket strengths, according to the  $s$ -process spread observed in disc stars and in presolar meteoritic SiC grains. The  $r$  contribution was assumed to derive from SNeII of 8–10  $M_\odot$ . Nevertheless we do not exclude different hypotheses to explore the chemical origin of the Galactic halo (e.g., see discussion in Section 1). The LEPP contribution was evoked to explain the missing abundance of solar Sr; the at  $[\text{Sr}/\text{Fe}]$  trend observed at low metallicities suggested that LEPP is a primary process, likely occurring in CCSNe with an extended range of mass progenitors compared to the main  $r$ -process. In Fig. 4, the Galactic disc predictions by Travaglio et al. (2004) are represented by black line for thin disc and dashed black line for thick disc. Note that the models which consider only the contribution in neutron-capture enrichment from  $s$ - and  $r$ -processes do not reproduce the observations at low metallicity (black dotted line).

In Figs. 4, 5, GCE calculations by Bisterzo et al. (2017) are compared with the observations (thin disc - blue line, thick disc - blue dotted line). Bisterzo et al. (2017) simulations included new stellar yields and GCE parameters set compared to Travaglio et al. (2004). In particular, GCE Fe predictions by Bisterzo et al. (2017) are obtained by using SNIa stellar yields by (Travaglio, Hillebrandt & Reinecke 2005), coupled with an updated treatment of the delayed-time distribution function as suggested by Kobayashi et al. (1998), Kobayashi, Nomoto & Hachisu (2015), Greggio (2005), Matteucci et al. (2009), in which we assume a dominant SNIa contribution starting from  $[\text{Fe}/\text{H}] > -1$ .

Bisterzo et al. (2017) also investigate the impact on GCE simulations of the internal structure of the  $^{13}\text{C}$  pocket, that is one of the major uncertainties for the  $s$ -process production in AGB stars. Considering these uncertainties, the authors confirmed their earlier results (Travaglio et al. 2004), where an additional LEPP contribution is required in order to represent the solar  $s$ -process abundances of isotopes from  $A = 90$  to 130 (solar LEPP, Montes et al. 2007). Bisterzo et al. (2017) also discussed the impact of the  $s$ -process yields from fast-rotating massive stars, with a contribution up to  $\sim 17\%$  to solar Sr ( $s$ -process yields from fast-rotating massive stars yields by Frischknecht et al. 2016). Therefore, according to those calculations, the maximum  $s$ -process production of Sr is  $\text{Sr}_s \sim 90\%$ . Instead,  $s$ -process isotopes and elements with  $90 < A < 130$  are marginally affected by this additional source of  $s$ -process, with variations within the solar uncertainties.

GCE simulations presented in the figure can reproduce Sr production in the galaxy and the solar abundances of Sr. In particular, by considering also the contribution from fast-rotating massive stars the  $[\text{Sr}/\text{Fe}]$  abundance in thin-disc stars is better reproduced compared to Travaglio et al. (2004). On the other hand, the production of Y and heavier

LEPP elements is not obtained, possibly made by a combination of other nucleosynthesis processes.

In Fig. 6 we show the evolution of the  $[\text{Sr}/\text{Ba}]$  and  $[\text{Sr}/\text{Eu}]$  ratios with respect to  $[\text{Fe}/\text{H}]$ . The average observational error is reported in the figures. The abundances for Ba and Eu were taken from Mishenina et al. (2013). Ba abundances were computed under the NLTE approximation in our earlier studies (Korotin et al. 2011; Mishenina et al. 2013). Ba abundances in dwarf stars were determined from Ba II 4554, 5853, 6141 and 6496 Å while the LTE Eu abundance was derived from the line at 6645 Å (Mishenina et al. 2013). The NLTE profiles of the Ba lines were computed using a modified version of the MULTI code (Carlsson 1986); all modifications have been described in detail in (Korotin, Andrievsky & Luck 1999). The Ba model in this study contains 31 levels of Ba I, 101 levels of Ba II with  $n < 50$  and the ground level of the Ba III. The analysis covers 91 bound-bound transitions. The NLTE Ba calculations have been described in detail in (Korotin et al. 2011). In order to verify the effect of the LTE deviations on the Sr abundance, as well as on their relationship with other elemental abundances, we have plotted  $[\text{Sr}/\text{Eu}]$  vs  $[\text{Fe}/\text{H}]$  using both the NLTE and LTE Sr abundances. As can be seen in Fig. 6, there is no significant difference. A pure  $r$ -process signature has been indicated for both  $[\text{Sr}/\text{Ba}]$  and  $[\text{Sr}/\text{Eu}]$  assuming that  $\text{Sr}_r = 9\%$  of the solar Sr abundance. This estimation is based on observations of very metal-poor  $r$ -process rich stars (Travaglio et al. 2004; Mashonkina & Christlieb 2014; Roederer et al. 2014). We use then  $\text{Ba}_r = 15\%$  of the solar Ba content and  $\text{Eu}_r = 94\%$  of the solar Eu abundance (using the residual method and the GCE  $s$ -process calculations by Bisterzo et al. 2017). The  $r$ -process contribution to Ba and Eu in the solar composition are derived by subtracting the  $s$ -process fractions from the solar abundances ( $r$ -process residuals method).

The  $[\text{Sr}/\text{Eu}]_r$  ratio is well below any star observed in the Galactic disc, confirming that other early nucleosynthesis processes producing Sr are contributing. The  $[\text{Sr}/\text{Ba}]_r$  ratio is close to the solar ratio, and not much information can be derived. In Fig. 7, the  $[\text{Sr}/\text{Ba}]$  (NLTE) ratio is shown with respect to the  $[\text{Ba}/\text{Eu}]$  (NLTE Ba, LTE Eu) ratio. Ratios consistent with the  $r$ -process production and the  $s$ -process contribution are shown for comparison. Most of the stars show abundance signatures consistent with a combined contribution of  $s$ -process and  $r$ -process. Also in the Galactic disc, we can see for a number of stars a possible signature similar to the stellar LEPP (Montes et al. 2007), where the  $[\text{Sr}/\text{Ba}]$  is larger than the  $s$ -process contributions and the  $r$ -process, and consistent with François et al. (2007) results, where an anti-correlations of  $[\text{Sr}/\text{Ba}]$ ,  $[\text{Y}/\text{Ba}]$  and  $[\text{Zr}/\text{Ba}]$  ratios with  $4.5 < [\text{Ba}/\text{H}] < 1.5$  was obtained. These results confirm the need of additional nucleosynthesis processes responsible for the synthesis of the first-peak elements. Andrievsky et al. (2011) have reanalyzed in NLTE approximation Sr and Ba abundances from François et al. (2007) and have compared with the theoretical predictions of the LEPP model (Travaglio et al. 2004). Their NLTE homogeneous determinations qualitatively confirm Sr, Y, Zr, Ba behaviour found in François et al. (2007), and enable one to robustly claim that the Sr abundances are generally higher than those predicted by the main  $r$ -process pattern. They have concluded that since the theoretical curve of a

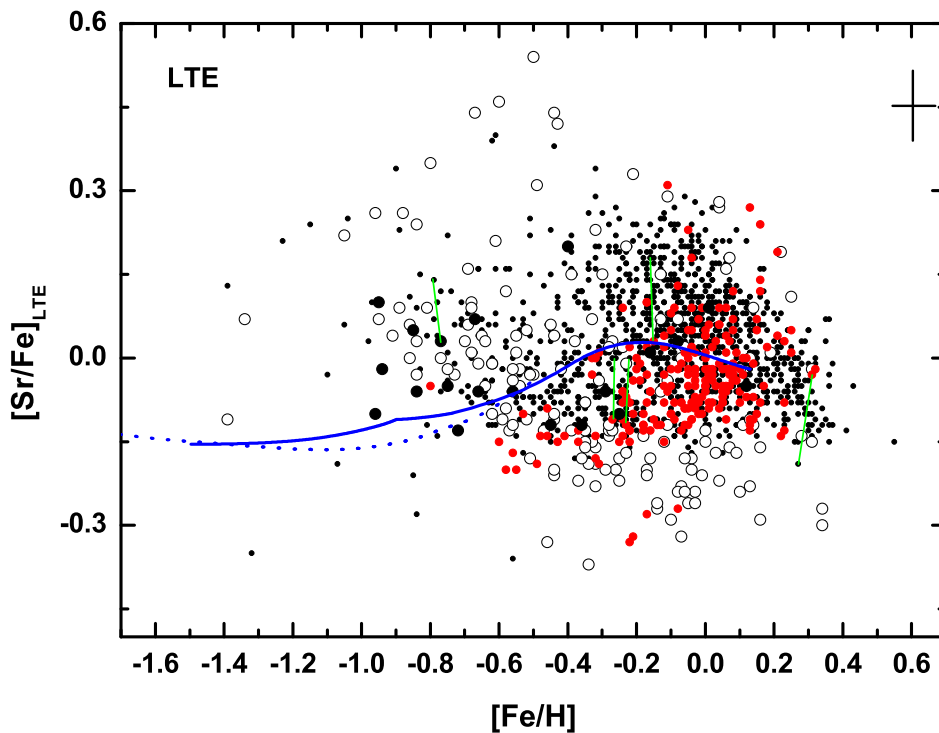


**Figure 5.** A comparison of our  $[\text{Sr}/\text{Fe}]_{\text{LTE}}$  (thin disc - red circles, thick disc - black circles) with the data of Battistini & Bensby (2016) (open circles), Delgado Mena et al. (2017) (points) and the chemical evolution prediction by Bisterzo et al. (2017) (thin disc - blue line, thick disc - dotted blue line). The values of the Sr abundance obtained by us and in other works that are different by more than 0.1 dex are connected (marked) by green lines.

LEPP process is not far from the upper envelope of their data points, then an inhomogeneous mixing of the products of such a LEPP process with the products of the main  $r$ -process could explain the distribution of studied metal-poor stars. In our figures, the stars with highest  $[\text{Sr}/\text{Ba}]$  are less than 0.3 dex beyond the  $s$ -process prediction. This might be seen as a signature of the different nucleosynthesis processes contributing to Sr and discussed before for Galactic Archaeology studies, but this scatter is close to the  $[\text{Sr}/\text{Ba}]$  observational error. Four stars have a ratio of  $[\text{Sr}/\text{Ba}]$  (Sr and Ba abundances presented in NLTE approach) higher than 0.3 dex, namely HD64606 ( $[\text{Sr}/\text{Fe}] = 0.17$ ,  $[\text{Sr}/\text{Ba}] = 0.31$ ), HD139323 ( $[\text{Sr}/\text{Fe}] = 0.32$ ,  $[\text{Sr}/\text{Ba}] = 0.32$ ), HD144579 ( $[\text{Sr}/\text{Fe}] = 0.11$ ,  $[\text{Sr}/\text{Ba}] = 0.37$ ) (Hercules stream) and one HD32147 ( $[\text{Sr}/\text{Fe}] = 0.28$ ,  $[\text{Sr}/\text{Ba}] = 0.32$ ) belongs to unclassified stars. These stars have a different kinematics from the stars of thick and thin discs and this could give an occasion to consider their special enrichment with Sr. However, only two of them show some excess of Sr, slightly exceeding the determination errors. Interestingly, there are five stars with the  $[\text{Sr}/\text{Ba}]$  ratio falling outside the range of errors from  $s$ -process or  $r$ -process: HD 26923 ( $[\text{Sr}/\text{Ba}] = -0.249$  LTE, 0.03 NLTE), HD45088 (-0.309, -0.269), HD53927 (-0.259, -0.279), HD127506 (-0.191, -0.231), HD141272 (-0.187, -0.047). The  $[\text{Sr}/\text{Ba}]$  ratios for each star are given in parentheses wherein the first value corresponds to the LTE Sr abundance and the

second value corresponds to the NLTE Sr content; for Ba the NLTE abundance estimates are used in both cases. For three stars, HD45088, 53927 and 127506, these deviations are the same for both the LTE and NLTE Sr abundance determinations. Again, we are quite close to the error range limit. The same uncommon signature is observed in few metal poor stars (e.g., Roederer et al. 2010; Frebel 2010; Hansen et al. 2018), indicating the contribution from different  $r$ -process components or some additional nucleosynthesis component which is not taken into account in this analysis.

In Figure 8 we have compared our  $[\text{Sr}/\text{Fe}]$  LTE data and those obtained in numerous studies within a large range of  $[\text{Fe}/\text{H}]$ , with GCE predictions by Bisterzo et al. (2017) and Prantzos et al. (2018). The computed evolution from Bisterzo et al. (2017) marked for thin disc as blue line and thick disc as dotted blue line (Fig. 8). The predicted evolution (Prantzos et al. 2018) is shown for the cases wherein different contributing sources were considered: i) low and intermediate mass (LIM) stars, rotating massive stars plus their fiduciary  $r$ -process (the baseline model, orange continuous curve); ii) LIM stars, non-rotating massive stars and  $r$ -process (green dashed curve); iii) LIM stars and non-rotating massive stars without  $r$ -process contribution (gray dashed curve); and iv) LIM stars plus rotating massive stars without the  $r$ -process contribution (orange dashed curve). The authors have drawn the conclusion that overall the computed

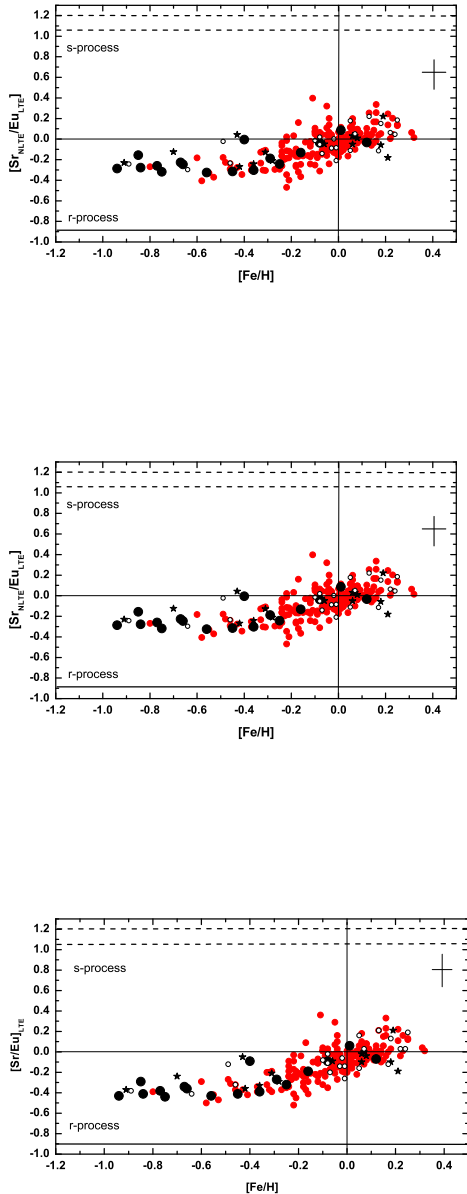


**Figure 6.** Dependencies of  $[Sr/Ba]$  (NLTE),  $[Sr/Eu]$  (Sr NLTE data) and  $[Sr/Eu]$  (Sr LTE data) vs.  $[Fe/H]$  with  $r$ -,  $s$ - process introduction from Bisterzo et al. (2017). The  $s$ -process signatures (pure AGB  $s$ -process production and including  $s$ -process contribution from massive stars) and  $r$ -process signatures are included:  $[Sr/Ba]_r = -0.10$ ;  $[Sr/Eu]_r = -0.89$ ;  $[Ba/Eu]_r = -0.80$ ;  $[Sr/Ba]_s = -0.09$  (pure AGB)-  $+0.05$  (AGB + massive stars);  $[Sr/Eu]_s = 1.06$  (pure AGB) -  $1.20$ (AGB + massive stars);  $[Ba/Eu]_s = 1.15$ . Notations are: thin disc stars marked as red circles, thick disc stars – as black circles, Hercules stream stars – as asterisks, non-classified stars – as small open circles;  $r$ -process as solid line,  $s$ -process as dotted lines.

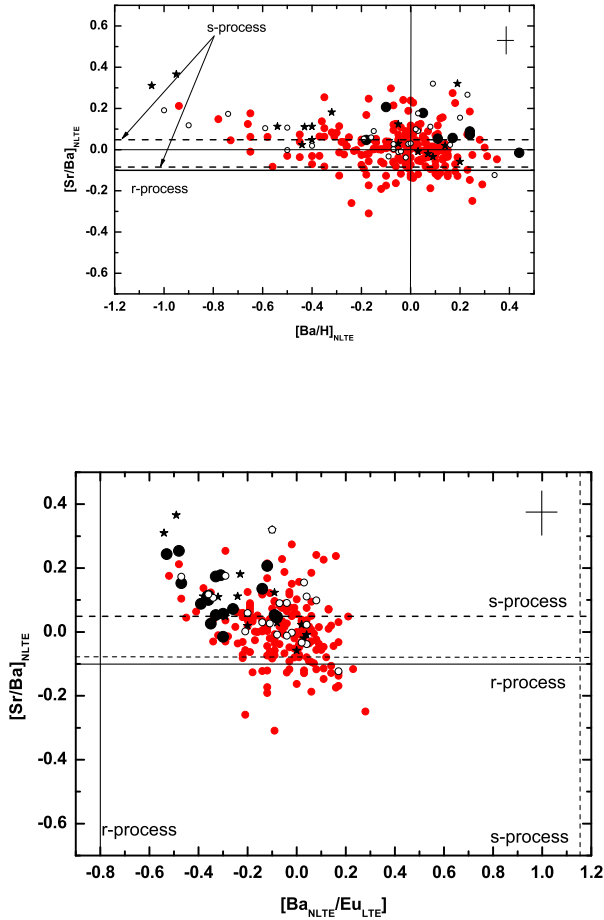


**Figure 7.** The  $[Sr/Ba]$  ratio (NLTE Sr, Ba) is shown with respect to  $[Ba/H]$  (NLTE Ba) and  $[Ba/Eu]$  (NLTE Ba, LTE Eu with  $r$ -,  $s$ - process introduction from Bisterzo et al. (2017)). Notations are the same as in Fig. 6.

$[X/Fe]$  vs.  $[Fe/H]$  evolution for the  $s$ -elements is consistent with the evolution predictions made in the previous studies (e.g. Bisterzo et al. 2017) for metallicities typical of the disc ( $[Fe/H] \geq -1.0$ ), but the weak  $s$ -process in rotating massive stars plays a key role in the evolution of the  $s$ -elements at low metallicity. Note the extra source of neutron-capture elements required to explain the solar abundances which led Travaglio et al. (2004) to postulate as additional process (LEPP) could apparently be explained by Prantzos et al. (2018) as a contribution from rotating massive stars.

As can be seen in the figures, there is a large scatter of Sr abundances at all metallicities, including the near-solar ones, which are of specific interest in this study. The resulting spread exceeds the observation errors, as well as the differences obtained in various studies applying different approaches (e.g. using the LTE or NLTE assumptions). In order to evaluate the description of the observational data by various calculations (using different models) of GCE, we have presented our observations and those obtained by Battistini & Bensby (2016) and Delgado Mena et al. (2017) as a single data set and expressed them as a third degree polynomial to plot versus the average observational

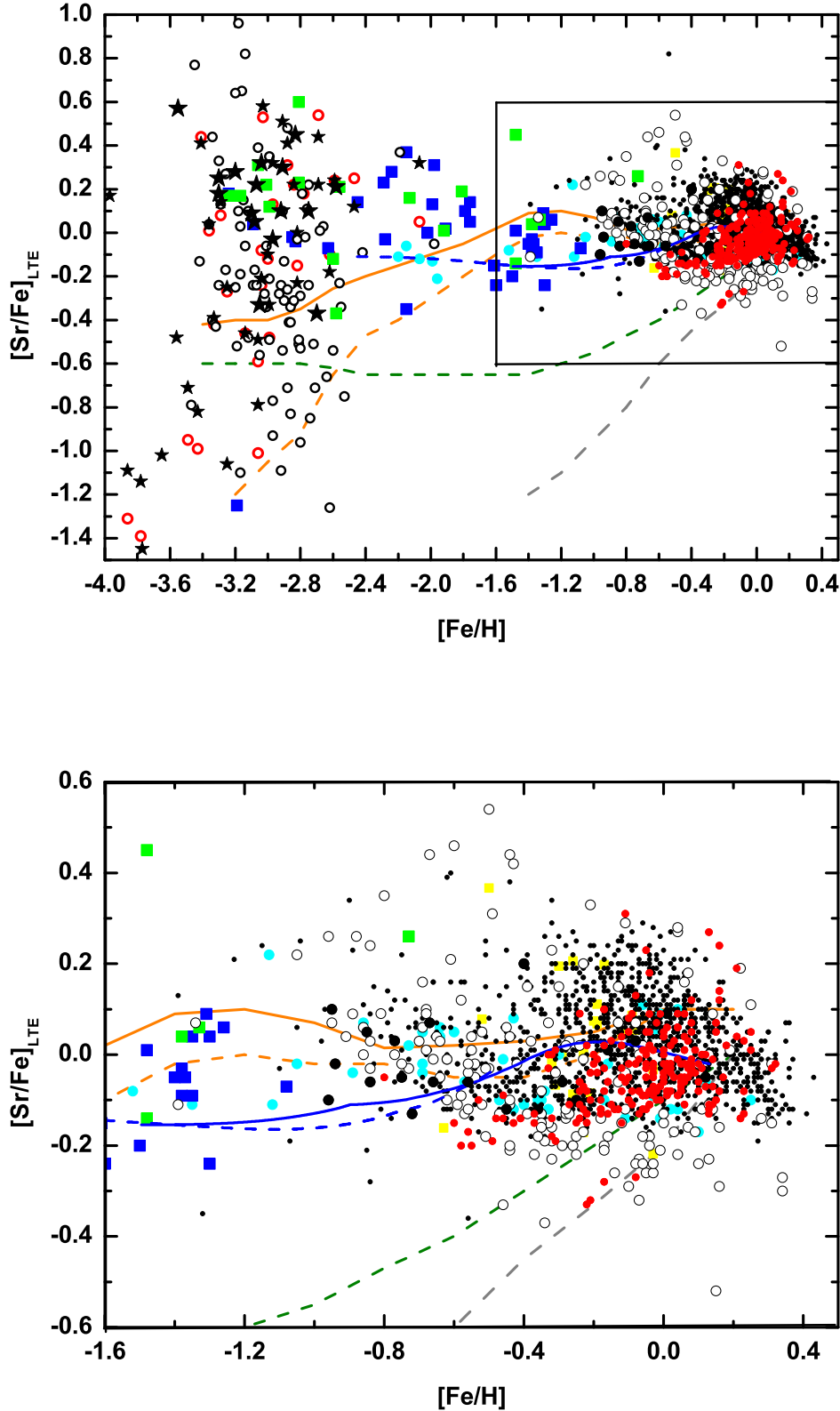


**Figure 8.** A comparison of our  $[\text{Sr}/\text{Fe}]_{\text{LTE}}$  data and those of other works with GCE predictions with the chemical evolution prediction by Bisterzo et al. (2017) and Prantzos et al. (2018) (see model details in text). The data from different literature sources are marked as follows: our thin disc data - as small red circles, our thick disc data - as black circles; data from Mashonkina & Gehren (2001) - as black circles; data from Brewer & Carney (2006) - as cyan circles; data from François et al. (2007) - as big red open circles, data from

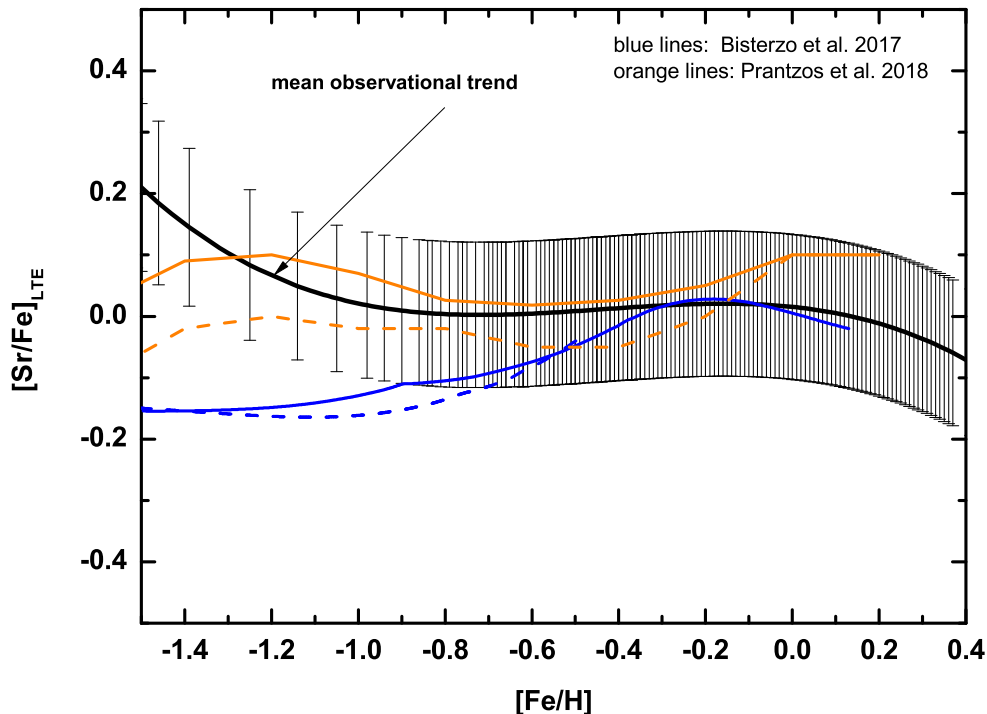


**Figure 9.** A comparison of the average observational  $[\text{Sr}/\text{Fe}]_{\text{LTE}}$  data trend with the chemical evolution prediction by Bisterzo et al. (2017) and Prantzos et al. (2018) and in Galactic disc range of  $[\text{Fe}/\text{H}]$ .

trend. Fig. 9 illustrates the average observational trend with the error function determination by a polynomial, as well as models developed by Bisterzo et al. (2017) and Prantzos et al. (2018). We have displayed the predicted evolution of Bisterzo et al. (2017) (for thin disc as blue line and thick disc as dotted blue line) and those of Prantzos et al. (2018) for the cases wherein different contributing sources were considered: a) low and intermediate mass (LIM) stars, rotating massive stars and  $r$ -process contribution (the baseline model, orange continuous curve); b) LIM stars plus rotating massive stars without the  $r$ -process contribution (orange dashed curve). Indeed the computed  $[\text{Sr}/\text{Fe}]$  vs.  $[\text{Fe}/\text{H}]$  evolution is well consistent with the predictions made by Bisterzo et al. (2017) and Prantzos et al. (2018) for metallicities typical for the disc stars ( $[\text{Fe}/\text{H}] \geq -1.0$ ). The main difference between the adopted models is due to the different contribution from massive rotating stars to the chemical enrichment. However, differences in the Sr abundance evolution in these two models are still within the accuracy of observations.

## 5 CONCLUSIONS

We present a new set of the Sr abundances measured for 276 stars, including 212 thin disc stars, 21 thick disc stars, 16 Hercules stream stars and 27 non-classified stars. By the time this study began, the Sr abundances had been deter-

mined for less than 2% of the stars in our sample. The LTE approach was employed to estimate the abundances, whereby the departures from LTE were determined using the results of Bergemann et al. (2012); the average NLTE correction was 0.15 dex. Comparison of our data with those of other authors showed good agreement between them, with only five stars with a departure in the  $[\text{Sr}/\text{Fe}]$  by more than 0.05 dex.

We obtain an observational scatter in the Sr abundance in the order of 0.2 – 0.3 dex is measured, beyond observational errors (0.12 – 0.17 dex, see Table 3), in agreement with previous works. For thin disc stars we obtain a scatter  $-0.28 \lesssim [\text{Sr}/\text{Fe}] \lesssim 0.34$ , which is higher than the same range measured for more metal-poor thick-disc stars (from  $-0.03 \lesssim [\text{Sr}/\text{Fe}] \lesssim 0.26$  dex). However, our sample of thick disc stars is too limited to draw robust conclusions. No significant trend is observed for the  $[\text{Sr}/\text{Fe}]$  evolution with respect to  $[\text{Fe}/\text{H}]$ . We note that there is no significant difference between the LTE and NLTE trends as can be seen in Fig. 6.

We compared our results with the GCE calculations by Travaglio et al. (2004), Bisterzo et al. (2017) and Prantzos et al. (2018). A number of stellar sources contributed to the production of Sr in stars. We considered the  $s$ -process contribution from AGB stars, from massive stars and from fast-rotating massive stars. The  $\text{Sr}_s$  ranges from 69% of the solar Sr due to AGB stars, up to  $\sim 90\%$  where also massive star contribution is taken into account. Based on observations of metal-poor  $r$ -process rich stars,

the contribution to the solar Sr from the  $r$ -process is smaller than 10%. The LEPP contribution was evoked to explain the missing abundance of solar Sr; the  $[\text{Sr}/\text{Fe}]$  trend observed at low metallicities suggested that LEPP is a primary process, likely occurring in CCSNe with an extended range of mass progenitors compared to the main  $r$ -process.

We have explored the Sr production together with Ba and Eu. We showed that while most of the stars can be explained within the  $s$ -process and  $r$ -process residual paradigm, there is a fraction of stars with  $[\text{Sr}/\text{Ba}]$  higher than the upper limit of Sr  $s$ -process contribution. While this feature is quite common in old stars formed in the early Galaxy, the observed departure from the  $s$ -process limit of  $[\text{Sr}/\text{Fe}]$  is much weaker in Galactic disc stars, within the observational errors ( $\sim 0.2$  dex). We obtain also a small fraction of stars with  $[\text{Sr}/\text{Ba}]$  lower by up to 0.2 dex than the  $r$ -process. At least for three stars, both LTE and NLTE Sr abundances display the values near -0.3 dex. Of course, taking into account the determination errors, this value is not so large, somewhere around 0.1 dex, which may be due to the dispersion of strontium and barium in the disc.

Using stellar data from our sample, from Battistini & Bensby (2016) and Delgado Mena et al. (2017) we have studied the production of Sr. Observations have been compared with GCE simulations by Bisterzo et al. (2017) and Prantzos et al. (2018). We confirm that the  $s$ -process contribution from the AGB stars, massive stars and fast-rotating massive stars is the main source of the Sr enrichment in the Galactic disc, possibly augmented by a CCSN contribution. The contribution of the fast-rotating massive stars becomes more significant with decreasing metallicity.

A significant scatter in the  $[\text{Sr}/\text{Fe}]$  ratio is also seen in metal-poor stars, possibly indicating the contribution from additional  $r$ -process components in the early Galaxy (e.g. a main  $r$ -process contribution from rare events at low metallicities) and in the Galactic disc.

## ACKNOWLEDGEMENTS

We thank Elisa Delgado Mena for providing the data before the publishing. TM, TG, MP, FKT and SK thank for the support from the Swiss National Science Foundation, project SCOPES No. IZ73Z0152485. MP acknowledges significant support to NuGrid from NSF grants PHY 09-22648 (Joint Institute for Nuclear Astrophysics, JINA), NSF grant PHY-1430152 (JINA Center for the Evolution of the Elements) and EU MIRG-CT-2006-046520. MP acknowledges the support from the "Lendlet-2014" Programme of the Hungarian Academy of Sciences (Hungary), from SNF (Switzerland), from STFC (UK, through the University of Hull Consolidated Grant ST/R000840/1) and from VIPER HPC facility at the University of Hull (UK). FKT acknowledges support from the European Research Council (FP7) under ERC Advanced Grant Agreement 321263 FISH. SB thanks JINA (ND Fund 202476) for financial support. TM thanks to O. Chepizhko for discussions. Authors are thankful to the anonymous referee for her/his very useful comments.

## REFERENCES

- Allende Prieto C., García López R. J., Lambert D. L., Gustafsson B., 1999, *ApJ*, 527, 879
- Andrievsky S. M., Spite F., Korotin S. A., François P., Spite M., Bonifacio P., Cayrel R., Hill V., 2011, *A&A*, 530, A105
- Aoki W., Beers T. C., Christlieb N., Norris J. E., Ryan S. G., Tsangarides S., 2007, *ApJ*, 655, 492
- Aoki W. et al., 2013, *AJ*, 145, 13
- Arcones A., Montes F., 2011, *ApJ*, 731, 5
- Asplund M., Grevesse N., Sauval A. J., Scott P., 2009, *ARA&A*, 47, 481
- Battistini C., Bensby T., 2016, *A&A*, 586, A49
- Belyakova E. V., Mashonkina L. I., 1997, *Astronomy Reports*, 41, 530
- Bergemann M., Hansen C. J., Bautista M., Ruchti G., 2012, *A&A*, 546, A90
- Bisterzo S., Travaglio C., Gallino R., Wiescher M., Käppeler F., 2014, *ApJ*, 787, 10
- Bisterzo S., Travaglio C., Wiescher M., Käppeler F., Gallino R., 2017, *ApJ*, 835, 97
- Brewer M.-M., Carney B. W., 2006, *AJ*, 131, 431
- Burris D. L., Pilachowski C. A., Armandroff T. E., Sneden C., Cowan J. J., Roe H., 2000, *ApJ*, 544, 302
- Carlsson M., 1986, *Uppsala Astronomical Observatory Reports*, 33
- Castelli F., Kurucz R. L., 2004, *ArXiv Astrophysics e-prints*, astro-ph/0405087
- Cescutti G., Chiappini C., Hirschi R., Meynet G., 2015a, *IAU General Assembly*, 22, 2257239
- Cescutti G., Romano D., Matteucci F., Chiappini C., Hirschi R., 2015b, *A&A*, 577, A139
- Chopin A., Ekström S., Meynet G., Maeder A., Georgy C., Hirschi R., 2017, *A&A*, 605, A63
- Clarkson O., Herwig F., Pignatari M., 2018, *MNRAS*, 474, L37
- Cowan J. J., Rose W. K., 1977, *ApJ*, 217, 51
- Cowan J. J., Sneden C., Lawler J. E., Aprahamian A., Wiescher M., Langanke K., Martínez-Pinedo G., Thielemann F.-K., 2019, *arXiv e-prints*, 1901.01410
- Cristallo S., Abia C., Straniero O., Piersanti L., 2015, *ApJ*, 801, 53
- Curtis S., Ebinger K., Fröhlich C., Hempel M., Perego A., Liebendörfer M., Thielemann F.-K., 2019, *ApJ*, 870, 2
- Dardelet L. et al., 2014, in *XIII Nuclei in the Cosmos (NIC XIII)*, p. 145
- Delgado Mena E., Tsantaki M., Adibekyan V. Z., Sousa S. G., Santos N. C., González Hernández J. I., Israelian G., 2017, *A&A*, 606, A94
- D’Orazi V., De Silva G. M., Melo C. F. H., 2017, *A&A*, 598, A86
- Eichler M. et al., 2017, in *14th International Symposium on Nuclei in the Cosmos (NIC2016)*, Kubono S., Kajino T., Nishimura S., Isobe T., Nagataki S., Shima T., Takeda Y., eds., p. 020604
- Farouqi K., Kratz K.-L., Mashonkina L. I., Pfeiffer B., Cowan J. J., Thielemann F.-K., Truran J. W., 2009, *ApJ*, 694, L49
- François P. et al., 2007, *A&A*, 476, 935
- Frebel A., 2010, *Astronomische Nachrichten*, 331, 474
- Freiburghaus C., Rosswog S., Thielemann F.-K., 1999,

- ApJ, 525, L121
- Friskhnecht U. et al., 2016, MNRAS, 456, 1803
- Fröhlich C., Hix W. R., Martínez-Pinedo G., Liebendörfer M., Thielemann F.-K., Bravo E., Langanke K., Zinner N. T., 2006, New Astr. Rev., 50, 496
- Fujiya W., Hoppe P., Zinner E., Pignatari M., Herwig F., 2013, ApJ, 776, L29
- Gaia Collaboration et al., 2018, A&A, 616, A11
- Galazutdinov G. A., 1992, Preprint SAO RAS, 92
- Gibson B. K., Fenner Y., Renda A., Kawata D., Lee H.-c., 2003, PASA, 20, 401
- Goswami A., Prantzos N., 2000, A&A, 359, 191
- Gratton R. G., Carretta E., Castelli F., 1996, A&A, 314, 191
- Greggio L., 2005, A&A, 441, 1055
- Grevesse N., Scott P., Asplund M., Sauval A. J., 2015, A&A, 573, A27
- Hampel M., Stancliffe R. J., Lugaro M., Meyer B. S., 2016, ApJ, 831, 171
- Hansen C. J., Bergemann M., Cescutti G., François P., Arcones A., Karakas A. I., Lind K., Chiappini C., 2013, A&A, 551, A57
- Hansen C. J., Montes F., Arcones A., 2014, ApJ, 797, 123
- Hansen T. T. et al., 2018, ApJ, 858, 92
- Herwig F., Pignatari M., Woodward P. R., Porter D. H., Rockefeller G., Fryer C. L., Bennett M., Hirschi R., 2011, ApJ, 727, 89
- Honda S., Aoki W., Ishimaru Y., Wanajo S., 2007, ApJ, 666, 1189
- Honda S., Aoki W., Kajino T., Ando H., Beers T. C., Izumiura H., Sadakane K., Takada-Hidai M., 2004, ApJ, 607, 474
- Ishigaki M. N., Aoki W., Chiba M., 2013, ApJ, 771, 67
- Käppeler F., Gallino R., Bisterzo S., Aoki W., 2011, Reviews of Modern Physics, 83, 157
- Karakas A. I., Lattanzio J. C., 2014, PASA, 31, e030
- Katz D., Soubiran C., Cayrel R., Adda M., Cautain R., 1998, A&A, 338, 151
- Kobayashi C., Karakas A. I., Umeda H., 2011, MNRAS, 414, 3231
- Kobayashi C., Nomoto K., Hachisu I., 2015, ApJ, 804, L24
- Kobayashi C., Tsujimoto T., Nomoto K., Hachisu I., Kato M., 1998, ApJ, 503, L155
- Korotin S., Mishenina T., Gorbaneva T., Soubiran C., 2011, MNRAS, 415, 2093
- Korotin S. A., Andrievsky S. M., Luck R. E., 1999, A&A, 351, 168
- Kovtyukh V. V., Soubiran C., Belik S. I., Gorlova N. I., 2003, A&A, 411, 559
- Kupka F., Piskunov N.E., Ryabchikova T.A., Stempels H. C., Weiss W. W., 1999, A&AS, 138
- Liu N. et al., 2014, ApJ, 786, 66
- Martínez-Pinedo G., Fischer T., Huther L., 2014, Journal of Physics G Nuclear Physics, 41, 044008
- Mashonkina L., Christlieb N., 2014, A&A, 565, A123
- Mashonkina L., Gehren T., 2001, A&A, 376, 232
- Mashonkina L., Gehren T., Shi J.-R., Korn A. J., Grupp F., 2011, A&A, 528, A87
- Matteucci F., Greggio L., 1986, A&A, 154, 279
- Matteucci F., Spitoni E., Recchi S., Valiante R., 2009, A&A, 501, 531
- Meynet G., Maeder A., 2017, Supernovae from Rotating Stars, Alsabti A. W., Murdin P., eds., p. 601
- Mishenina T. et al., 2015, MNRAS, 446, 3651
- Mishenina T. V., Kovtyukh V. V., 2001, A&A, 370, 951
- Mishenina T. V., Pignatari M., Korotin S. A., Soubiran C., Charbonnel C., Thielemann F.-K., Gorbaneva T. I., Basak N. Y., 2013, A&A, 552, A128
- Mishenina T. V., Soubiran C., Bienaymé O., Korotin S. A., Belik S. I., Usenko I. A., Kovtyukh V. V., 2008, A&A, 489, 923
- Mishenina T. V., Soubiran C., Kovtyukh V. V., Korotin S. A., 2004, A&A, 418, 551
- Montes F. et al., 2007, ApJ, 671, 1685
- Moultaka J., Ilovaisky S. A., Prugniel P., Soubiran C., 2004, PASP, 116, 693
- Nishimura N., Sawai H., Takiwaki T., Yamada S., Thielemann F.-K., 2017, ApJ, 836, L21
- Nishimura N., Takiwaki T., Thielemann F.-K., 2015, ApJ, 810, 109
- Pignatari M., Gallino R., Heil M., Wiescher M., Käppeler F., Herwig F., Bisterzo S., 2010, ApJ, 710, 1557
- Pignatari M., Gallino R., Meynet G., Hirschi R., Herwig F., Wiescher M., 2008, ApJ, 687, L95
- Pignatari M., Göbel K., Reifarth R., Travaglio C., 2016a, International Journal of Modern Physics E, 25, 1630003
- Pignatari M. et al., 2016b, ApJS, 225, 24
- Prantzos N., Abia C., Limongi M., Chieffi A., Cristallo S., 2018, MNRAS, 476, 3432
- Qian Y.-Z., Wasserburg G. J., 2001, ApJ, 559, 925
- Qian Y.-Z., Wasserburg G. J., 2008, ApJ, 687, 272
- Raiteri C. M., Busso M., Picchio G., Gallino R., 1991a, ApJ, 371, 665
- Raiteri C. M., Busso M., Picchio G., Gallino R., Pulone L., 1991b, ApJ, 367, 228
- Rauscher T., Dauphas N., Dillmann I., Fröhlich C., Fülöp Z., Gyürky G., 2013, Reports on Progress in Physics, 76, 066201
- Reddy B. E., Tomkin J., Lambert D. L., Allende Prieto C., 2003, MNRAS, 340, 304
- Roberts L. F., Woosley S. E., Hoffman R. D., 2010, ApJ, 722, 954
- Roederer I. U., Cowan J. J., Karakas A. I., Kratz K.-L., Lugaro M., Simmerer J., Farouqi K., Sneden C., 2010, ApJ, 724, 975
- Roederer I. U., Karakas A. I., Pignatari M., Herwig F., 2016, ApJ, 821, 37
- Roederer I. U., Preston G. W., Thompson I. B., Shectman S. A., Sneden C., Burley G. S., Kelson D. D., 2014, AJ, 147, 136
- Shchukina N., Trujillo Bueno J., 2001, ApJ, 550, 970
- Sneden C., Cowan J. J., Gallino R., 2008, ARA&A, 46, 241
- Soubiran C., Bienaymé O., Siebert A., 2003, A&A, 398, 141
- Spite F., Spite M., Barbuy B., Bonifacio P., Caffau E., François P., 2018, A&A, 611, A30
- Spite M., Spite F., Bonifacio P., Caffau E., François P., Sbordone L., 2014, A&A, 571, A40
- Surman R., McLaughlin G. C., Ruffert M., Janka H.-T., Hix W. R., 2008, ApJ, 679, L117
- Takahashi K., Witt J., Janka H.-T., 1994, A&A, 286, 857
- The L.-S., El Eid M. F., Meyer B. S., 2007, ApJ, 655, 1058
- Thévenin F., Idiart T. P., 1999, ApJ, 521, 753

- Thielemann F.-K., Eichler M., Panov I. V., Wehmeyer B., 2017, *Annual Review of Nuclear and Particle Science*, 67, 253
- Timmes F. X., Woosley S. E., Weaver T. A., 1995, *ApJS*, 98, 617
- Travaglio C., Gallino R., Arnone E., Cowan J., Jordan F., Sneden C., 2004, *ApJ*, 601, 864
- Travaglio C., Hillebrandt W., Reinecke M., 2005, *A&A*, 443, 1007
- Travaglio C., Rauscher T., Heger A., Pignatari M., West C., 2018, *ApJ*, 854, 18
- Trippella O., Busso M., Palmerini S., Maiorca E., Nucci M. C., 2016, *ApJ*, 818, 125
- Tsymbal V., 1996, in *Astronomical Society of the Pacific Conference Series*, Vol. 108, M.A.S.S., *Model Atmospheres and Spectrum Synthesis*, Adelman S. J., Kupka F., Weiss W. W., eds., p. 198
- Wanajo S., Janka H.-T., Kubono S., 2011, *ApJ*, 729, 46
- Wanajo S., Janka H.-T., Müller B., 2011, *ApJ*, 726, L15
- Wehmeyer B., Pignatari M., Thielemann F.-K., 2015, *MNRAS*, 452, 1970
- Winteler C., Käppeli R., Perego A., Arcones A., Vasset N., Nishimura N., Liebendörfer M., Thielemann F.-K., 2012, *ApJ*, 750, L22
- Woosley S. E., Wilson J. R., Mathews G. J., Hoffman R. D., Meyer B. S., 1994, *ApJ*, 433, 229
- Yong D. et al., 2013, *ApJ*, 762, 26

**APPENDIX A:**



Table A1: Stellar parameters and abundances of some n-capture elements. The obtained (LTE) Sr abundances, the NLTE corrections from Bergemann et al. (2012), the NLTE Ba and LTE Eu abundance, and stellar parameters Mishenina et al. (2013).

HD/BD	$T_{\text{eff}}$ , K	$\log g$	[Fe/H]	Vt	[Sr/Fe]LTE	$\text{corr}_{NLTE}$	[Sr/Fe]NLTE	[Ba/Fe]NLTE	[Eu/Fe]
thin									
166	5514	4.6	0.16	0.6	0.14	0.12	0.16	0.12	-0.09
1562	5828	4	-0.32	1.2	0	0.18	0.08	0	
1835	5790	4.5	0.13	1.1	0.27	0.14	0.31	0.04	0.06
3651	5277	4.5	0.15	0.6	0.07	0.11	0.08	-0.14	-0.08
4256	5020	4.3	0.08	1.1	0.12	0.11	0.13	-0.16	
4307	5889	4	-0.18	1.1	-0.12	0.17	-0.04	0.08	0.12
4614	5965	4.4	-0.24	1.1	-0.06	0.17	0.01	0.02	0.08
5294	5779	4.1	-0.17	1.3	0.1	0.17	0.17	0.15	0.01
6660	4759	4.6	0.08	1.4	0.05	0.11	0.06	-0.15	-0.03
7590	5962	4.4	-0.1	1.4	0.08	0.16	0.14	0.11	0.07
7924	5165	4.4	-0.22	1.1	-0.13	0.15	-0.07	-0.05	0.04
8648	5790	4.2	0.12	1.1	-0.07	0.14	-0.02	-0.04	-0.13
9407	5666	4.45	0.05	0.8	-0.07	0.14	-0.02	-0.02	-0.03
9826	6074	4	0.1	1.3	-0.08	0.15	-0.02	-0.02	
10086	5696	4.3	0.13	1.2	-0.13	0.14	-0.09	-0.06	-0.08
10307	5881	4.3	0.02	1.1	-0.04	0.15	0.01	-0.02	0.12
10476	5242	4.3	-0.05	1.1	0.01	0.14	0.05	0	-0.06
10780	5407	4.3	0.04	0.9	0.06	0.13	0.09	0.09	0.05
11007	5980	4	-0.2	1.1	-0.02	0.17	0.05	0.05	0.19
11373	4783	4.65	0.08	1	0.07	0.11	0.08	-0.04	-0.01
12846	5766	4.5	-0.24	1.2	-0.08	0.17	0.00	-0.04	0.16
13507	5714	4.5	-0.02	1.1	0.07	0.15	0.12	0.11	0.16
14374	5449	4.3	-0.09	1.1	0.09	0.15	0.14	0.02	0.13
16160	4829	4.6	-0.16	1.1	-0.13	0.14	-0.08	-0.19	0.28
17674	5909	4	-0.14	1.1	-0.12	0.17	-0.05	-0.03	-0.02
17925	5225	4.3	-0.04	1.1	0.18	0.13	0.21	0.03	0.08
18632	5104	4.4	0.06	1.4	0.04	0.12	0.06	-0.04	-0.04
18803	5665	4.55	0.14	0.8	-0.01	0.13	0.02	0	-0.02
19019	6063	4	-0.17	1.1	0.1	0.17	0.17	0.17	
19373	5963	4.2	0.06	1.1	-0.06	0.15	0.00	-0.03	0.03
20630	5709	4.5	0.08	1.1	-0.01	0.14	0.03	0.07	
22049	5084	4.4	-0.15	1.1	0.03	0.14	0.07	0.15	0.24
22484	6037	4.1	-0.03	1.1	-0.07	0.16	-0.01	0.03	0.02
22556	6155	4.2	-0.17	1.1	-0.03	0.17	0.04	0.04	0.21
24053	5723	4.4	0.04	1.1	0.06	0.14	0.10	0.11	0.1
24238	4996	4.3	-0.46	1	-0.14	0.18	-0.05	-0.12	0.18
24496	5536	4.3	-0.13	1.5	-0.12	0.16	-0.06	-0.12	0.1
25665	4967	4.7	0.01	1.2	-0.09	0.12	-0.06	-0.03	0.06
25680	5843	4.5	0.05	1.1	-0.02	0.15	0.03	0.05	0.02
26923	5920	4.4	-0.03	1	-0.03	0.16	0.03	0.28	0
28005	5980	4.2	0.23	1.1	0.03	0.14	0.07	0	-0.13
28447	5639	4	-0.09	1.1	-0.11	0.16	-0.05	0.03	0.13
29150	5733	4.3	0	1.1	-0.05	0.15	0.00	-0.03	0.04
29310	5852	4.2	0.08	1.4	-0.02	0.15	0.03	0.02	
29645	6009	4	0.14	1.3	-0.11	0.15	-0.06	-0.07	-0.1
30495	5820	4.4	-0.05	1.3	0.05	0.16	0.11	0.19	0.07
33632	6072	4.3	-0.24	1.1	-0.06	0.17	0.01	0.18	0.18
34411	5890	4.2	0.1	1.1	-0.06	0.15	-0.01	-0.01	-0.01
37008	5016	4.4	-0.41	0.8	-0.14	0.17	-0.06	-0.24	0.28
37394	5296	4.5	0.09	1.1	0.01	0.12	0.03	0.06	-0.02
38858	5776	4.3	-0.23	1.1	-0.12	0.17	-0.04	0.03	0.15
39587	5955	4.3	-0.03	1.5	-0.05	0.16	0.01	0.14	-0.03
40616	5881	4	-0.22	1.1	-0.13	0.17	-0.05	0.12	-0.04

Table A1: continued.

HD/BD	$T_{\text{eff}}$ , K	$\log g$	[Fe/H]	Vt	[Sr/Fe]LTE	corr <sub>NLTE</sub>	[Sr/Fe]NLTE	[Ba/Fe]NLTE	[Eu/Fe]
41330	5904	4.1	-0.18	1.2	-0.12	0.17	-0.05	0.01	0.22
41593	5312	4.3	-0.04	1.1	0.09	0.14	0.13	0.1	-0.07
42618	5787	4.5	-0.07	1	-0.08	0.16	-0.02	0.02	0.09
42807	5719	4.4	-0.03	1.1	-0.04	0.15	0.01	0.11	0.05
43587	5927	4.1	-0.11	1.3	-0.06	0.16	0.00	-0.04	0.15
43856	6143	4.1	-0.19	1.1	-0.04	0.17	0.03	0.15	0.18
43947	6001	4.3	-0.24	1.1	-0.14	0.17	-0.06	0.06	0.2
45088	4959	4.3	-0.21	1.2	-0.32	0.15	-0.27	0.04	0.13
47752	4613	4.6	-0.05	0.2	-0.05	0.13	-0.02	-0.02	0.1
48682	5989	4.1	0.05	1.3	-0.08	0.15	-0.02	-0.08	-0.08
50281	4712	3.9	-0.2	1.6	0	0.15	0.05	0	
50692	5911	4.5	-0.1	0.9	-0.1	0.16	-0.03	0.03	0.22
51419	5746	4.1	-0.37	1.1	-0.13	0.19	-0.04	-0.08	0.26
51866	4934	4.4	0	1	0	0.12	0.02	-0.07	0.02
53927	4860	4.64	-0.22	1.2	-0.33	0.15	-0.28	-0.02	0.19
54371	5670	4.2	0.06	1.2	0.01	0.14	0.05	-0.01	0.03
55575	5949	4.3	-0.31	1.1	-0.19	0.18	-0.10	0.02	0.2
58595	5707	4.3	-0.31	1.2	0.01	0.18	0.09	0.01	0.2
59747	5126	4.4	-0.04	1.1	0.05	0.13	0.08	0.09	0.02
61606	4956	4.4	-0.12	1.3	0.02	0.14	0.06	0.02	0.13
62613	5541	4.4	-0.1	1.1	-0.05	0.15	0.00	0	-0.06
63433	5693	4.35	-0.06	1.9	-0.09	0.16	-0.03	0.02	0.03
64468	5014	4.2	0	1.2	0.05	0.12	0.07	-0.17	
64815	5864	4	-0.33	1.1	0	0.18	0.08	0.07	0.32
65874	5936	4	0.05	1.3	-0.05	0.15	0.00	-0.07	-0.11
68638	5430	4.4	-0.24	1.1	-0.11	0.17	-0.04	0.05	0.08
70923	5986	4.2	0.06	1.1	-0.02	0.15	0.03	-0.06	-0.12
71148	5850	4.2	0	1.1	-0.05	0.15	0.00	-0.01	-0.06
72760	5349	4.1	0.01	1.1	0.06	0.13	0.09	0.04	0.05
72905	5884	4.4	-0.07	1.5	-0.01	0.16	0.05	0.11	0.01
73344	6060	4.1	0.08	1.1	-0.04	0.15	0.01	-0.02	-0.04
73667	4884	4.4	-0.58	0.9	-0.2	0.19	-0.10	-0.15	0.3
75732	5373	4.3	0.25	1.1	0.01	0.11	0.02	-0.13	-0.11
75767	5823	4.2	-0.01	0.9	-0.07	0.15	-0.01	0.04	
76151	5776	4.4	0.05	1.1	-0.06	0.15	-0.01	-0.03	-0.06
79969	4825	4.4	-0.05	1	-0.02	0.13	0.01		0.07
82106	4827	4.1	-0.11	1.1	0.31	0.13	0.34	0.11	-0.05
82443	5334	4.4	-0.03	1.3	0.01	0.14	0.05	0.13	0.12
87883	5015	4.4	0	1.1	-0.06	0.12	-0.03	-0.05	0.02
88072	5778	4.3	0	1.1	-0.04	0.15	0.01	-0.03	0.15
89251	5886	4	-0.12	1.1	-0.08	0.16	-0.01	0.05	0.16
89269	5674	4.4	-0.23	1.1	-0.07	0.17	0.00	0.03	0.2
91347	5931	4.4	-0.43	1.1	-0.15	0.19	-0.05	-0.02	0.22
94765	5077	4.4	-0.01	1.1	0.09	0.13	0.12	0.07	
95128	5887	4.3	0.01	1.1	-0.08	0.15	-0.02	-0.05	0
97334	5869	4.4	0.06	1.2	-0.05	0.15	0.00	0.13	-0.01
97658	5136	4.5	-0.32	1.2	-0.18	0.16	-0.11	-0.03	0.19
98630	6060	4	0.22	1.4	-0.14	0.14	-0.09	-0.09	-0.1
101177	5932	4.1	-0.16	1.1	-0.06	0.17	0.01	0.01	0.15
102870	6055	4	0.13	1.4	-0.11	0.15	-0.06	-0.03	-0.09
105631	5416	4.4	0.16	1.2	-0.08	0.12	-0.05	-0.02	-0.04
107705	6040	4.2	0.06	1.4	-0.11	0.15	-0.05	0.06	-0.05
108954	6037	4.4	-0.12	1.1	-0.05	0.17	0.02	0.11	0.06
109358	5897	4.2	-0.18	1.1	-0.13	0.17	-0.06	-0.05	0.04
110463	4950	4.5	-0.05	1.2	0	0.13	0.03	0.04	0.09
110833	5075	4.3	0	1.1	0.04	0.12	0.06	-0.04	
111395	5648	4.6	0.1	0.9	0.02	0.14	0.02	0.19	0.02
112758	5203	4.2	-0.56	1.1	0.17	0.19	-0.07	-0.22	
114710	5954	4.3	0.07	1.1	0.05	0.15	0.00	0.11	-0.03

Table A1: continued.

HD/BD	$T_{\text{eff}}$ , K	$\log g$	[Fe/H]	Vt	[Sr/Fe]LTE	corr <sub>NLTE</sub>	[Sr/Fe]NLTE	[Ba/Fe]NLTE	[Eu/Fe]
115383	6012	4.3	0.11	1.1	0.03	0.15	0.02	0.12	0.05
115675	4745	4.45	0.02	1	0.02	0.12	0.00	-0.07	0.03
116443	4976	3.9	-0.48	1.1	0.14	0.18	-0.05	-0.18	0.17
116956	5386	4.55	0.08	1.2	0.03	0.13	0.00	0.05	0.04
117043	5610	4.5	0.21	0.4	0.04	0.13	0.07	0.1	-0.07
119802	4763	4	-0.05	1.1	0.23	0.13	0.26	0.02	-0.06
122064	4937	4.5	0.07	1.1	0.03	0.11	0.04	-0.07	0.07
124642	4722	4.65	0.02	1.3	-0.03	0.12	-0.01	-0.02	0.1
125184	5695	4.3	0.31	0.7	-0.03	0.12	-0.01	0.04	-0.07
126053	5728	4.2	-0.32	1.1	-0.14	0.18	-0.06	-0.13	0.06
127506	4542	4.6	-0.08	1.2	-0.27	0.14	-0.23	-0.04	0.08
128311	4960	4.4	0.03	1.3	0.03	0.12	0.05	-0.03	0.04
130307	4990	4.3	-0.25	1.4	-0.15	0.16	-0.09	0.08	0.2
130948	5943	4.4	-0.05	1.3	-0.03	0.16	0.03	0.15	0.07
131977	4683	3.7	-0.24	1.8	0.09	0.15	0.14	-0.11	0.18
135599	5257	4.3	-0.12	1	0.04	0.15	0.09	0.1	0.11
137107	6037	4.3	0	1.1	0.01	0.16	0.07	0.09	
139777	5771	4.4	0.01	1.3	-0.03	0.15	0.02	0.14	-0.09
139813	5408	4.5	0	1.2	-0.02	0.14	0.02	0.15	0.12
140538	5675	4.5	0.02	0.9	0.02	0.15	0.07	0.06	0.12
141004	5884	4.1	-0.02	1.1	-0.08	0.16	-0.02	0	0.11
141272	5311	4.4	-0.06	1.3	-0.09	0.14	-0.04	0.14	0.08
142267	5856	4.5	-0.37	1.1	-0.15	0.19	-0.06	-0.03	0.19
144287	5414	4.5	-0.15	1.1	-0.11	0.15	-0.05	-0.03	
145675	5406	4.5	0.32	1.1	-0.02	0.10	-0.01	-0.09	-0.03
146233	5799	4.4	0.01	1.1	-0.02	0.15	0.03	0.01	0.08
149661	5294	4.5	-0.04	1.1	0.02	0.14	0.06	0.01	0.03
149806	5352	4.55	0.25	0.4	0.05	0.11	0.06	0.05	-0.08
151541	5368	4.2	-0.22	1.3	-0.15	0.16	-0.08	-0.15	0.26
153525	4810	4.7	-0.04	1	-0.11	0.13	-0.08	0.04	0.16
154345	5503	4.3	-0.21	1.3	-0.1	0.17	-0.03	-0.05	0.15
156668	4850	4.2	-0.07	1.2	-0.13	0.13	-0.09	-0.13	0.05
156985	4790	4.6	-0.18	1	-0.1	0.14	-0.05	-0.09	0.2
158633	5290	4.2	-0.49	1.3	-0.19	0.19	-0.09	-0.16	0.08
160346	4983	4.3	-0.1	1.1	0.05	0.14	0.09	-0.08	0.04
161098	5617	4.3	-0.27	1.1	-0.11	0.17	-0.03	-0.02	0.26
164922	5392	4.3	0.04	1.1	-0.01	0.13	0.02	-0.1	0.1
165173	5505	4.3	-0.05	1.1	-0.12	0.15	-0.07	-0.07	0.09
165341	5314	4.3	-0.08	1.1	-0.02	0.14	0.02	0.03	0
165476	5845	4.1	-0.06	1.1	-0.12	0.16	-0.05	-0.06	
165670	6178	4	-0.1	1.5	-0.1	0.16	-0.03	0.1	
165908	5925	4.1	-0.6	1.1	-0.15	0.20	-0.04	0.04	0.14
166620	5035	4	-0.22	1	-0.08	0.15	-0.02	-0.09	0.16
171314	4608	4.65	0.07	1	-0.02	0.12	0.00	-0.09	0.1
174080	4764	4.55	0.04	1	0.09	0.12	0.11	-0.01	0.13
176377	5901	4.4	-0.17	1.3	-0.08	0.17	-0.01	0.05	0.14
176841	5841	4.3	0.23	1.1	-0.08	0.13	-0.04	-0.12	-0.09
178428	5695	4.4	0.14	1	-0.07	0.14	-0.03	0.04	0.03
180161	5473	4.5	0.18	1.1	0.02	0.12	0.04	0.07	-0.01
182488	5435	4.4	0.07	1.1	-0.03	0.13	0.00	-0.07	-0.03
183341	5911	4.3	-0.01	1.3	-0.1	0.16	-0.04	-0.08	0.1
184385	5536	4.45	0.12	0.9	0	0.13	0.03	0.07	-0.02
185144	5271	4.2	-0.33	1.1	-0.03	0.17	0.04	-0.02	0.17
185414	5818	4.3	-0.04	1.1	-0.11	0.16	-0.05	0.07	0.04
186408	5803	4.2	0.09	1.1	-0.04	0.15	0.01	-0.03	-0.05
186427	5752	4.2	0.02	1.1	-0.08	0.15	-0.03	-0.07	0.02
187897	5887	4.3	0.08	1.1	-0.03	0.15	0.02	0.03	
189087	5341	4.4	-0.12	1.1	-0.03	0.15	0.02	0.1	0.06
189733	5076	4.4	-0.03	1.5	-0.09	0.13	-0.06	-0.11	0.05

Table A1: continued.

HD/BD	$T_{\text{eff}}$ , K	$\log g$	[Fe/H]	Vt	[Sr/Fe]LTE	corr <sub>NLTE</sub>	[Sr/Fe]NLTE	[Ba/Fe]NLTE	[Eu/Fe]
190007	4724	4.5	0.16	0.8	0.12	0.10	0.12	-0.03	-0.04
190406	5905	4.3	0.05	1	-0.06	0.15	-0.01	0.05	-0.03
190470	5130	4.3	0.11	1	0	0.11	0.01	-0.08	0.01
190771	5766	4.3	0.13	1.5	-0.12	0.14	-0.08	-0.07	-0.06
191533	6167	3.8	-0.1	1.5	-0.02	0.16	0.04	0.09	-0.06
191785	5205	4.2	-0.12	1.2	-0.15	0.14	-0.10	-0.24	0.14
195005	6075	4.2	-0.06	1.3	0.01	0.16	0.07	0.06	
195104	6103	4.3	-0.19	1.1	-0.01	0.17	0.06	0.2	0.03
197076	5821	4.3	-0.17	1.2	0.02	0.17	0.09	0.08	0.21
199960	5878	4.2	0.23	1.1	-0.13	0.14	-0.09	-0.11	
200560	5039	4.4	0.06	1.1	0.09	0.12	0.11	0.04	-0.09
202108	5712	4.2	-0.21	1.1	-0.04	0.17	0.03	0.1	0.15
202575	4667	4.6	-0.03	0.5	-0.02	0.13	0.01	0.09	0.1
203235	6071	4.1	0.05	1.3	-0.08	0.16	-0.02	-0.05	-0.01
205702	6020	4.2	0.01	1.1	-0.03	0.16	0.03	-0.03	-0.02
206860	5927	4.6	-0.07	1.8	-0.08	0.16	-0.01	0.05	
208038	4982	4.4	-0.08	1	0.13	0.13	0.16	0.09	0.1
208313	5055	4.3	-0.05	1	-0.09	0.13	-0.05	-0.09	-0.03
208906	5965	4.2	-0.8	1.7	-0.05	0.22	0.07	-0.14	0.34
210667	5461	4.5	0.15	0.9	0.05	0.12	0.07	-0.04	-0.01
210752	6014	4.6	-0.53	1.1	-0.1	0.2	0.00	0.03	0.37
211472	5319	4.4	-0.04	1.1	0.02	0.14	0.06	0.1	
214683	4747	4.6	-0.46	1.2	-0.09	0.18	-0.01	0.06	0.28
216259	4833	4.6	-0.55	0.5	-0.2	0.19	-0.11	-0.1	0.22
216520	5119	4.4	-0.17	1.4	-0.28	0.15	-0.23	-0.2	0.09
217014	5763	4.3	0.17	1.1	-0.05	0.14	-0.01	-0.1	-0.05
217813	5845	4.3	0.03	1.5	-0.05	0.15	0.00	0.04	-0.01
218868	5547	4.45	0.21	0.4	0.19	0.12	0.21	0.03	-0.03
219538	5078	4.5	-0.04	1.1	-0.08	0.13	-0.04	-0.06	0.06
219623	5949	4.2	0.04	1.2	-0.09	0.15	-0.03	0.01	0.13
220182	5364	4.5	-0.03	1.2	-0.02	0.14	0.02	0.07	0.1
220221	4868	4.5	0.16	0.5	0.24	0.10	0.24	0.02	-0.09
221851	5184	4.4	-0.09	1	-0.08	0.14	-0.03	0.02	0.11
222143	5823	4.45	0.15	1.1	-0.1	0.14	-0.05	0.09	-0.02
224465	5745	4.5	0.08	0.8	-0.04	0.14	0.00	0.05	0.04
263175	4734	4.5	-0.16	0.5	-0.06	0.14	-0.02	-0.13	0.23
BD12063	4859	4.4	-0.22	0.6	0.02	0.15	0.07	0.07	0.05
BD124499	4678	4.7	0	0.5	0.04	0.12	0.06	0.02	0.24
thick disc									
245	5400	3.4	-0.84	0.7	-0.06	0.23	0.07	0.02	0.35
3765	5079	4.3	0.01	1.1	0.09	0.12	0.11	-0.09	0.03
5351	4378	4.6	-0.21	0.5	-	0.16	-	-0.33	0.08
6582	5240	4.3	-0.94	0.7	-0.02	0.24	0.12	-0.12	0.41
13783	5350	4.1	-0.75	1.1	-0.05	0.22	0.07	-0.08	0.39
18757	5741	4.3	-0.25	1	-0.1	0.17	-0.02	-0.08	0.22
22879	5972	4.5	-0.77	1.1	0.03	0.22	0.15	0.05	0.41
65583	5373	4.6	-0.67	0.7	0.07	0.21	0.18	-0.07	0.41
76932	5840	4	-0.95	1	0.1	0.23	0.23	0.1	
106516	6165	4.4	-0.72	1.1	-0.13	0.20	-0.02	0.09	
110897	5925	4.2	-0.45	1.1	-0.12	0.19	-0.02	-0.01	0.29
135204	5413	4	-0.16	1.1	0.01	0.15	0.06	-0.11	0.2
152391	5495	4.3	-0.08	1.3	0.03	0.15	0.08	0.03	0.12
157089	5785	4	-0.56	1	-0.06	0.20	0.04	0.02	0.37
157214	5820	4.5	-0.29	1	-0.06	0.18	0.02	-0.05	0.21
159062	5414	4.3	-0.4	1	0.2	0.18	0.28	0.15	0.29
165401	5877	4.3	-0.36	1.1	-0.12	0.18	-0.02	-0.12	0.27
190360	5606	4.4	0.12	1.1	-0.05	0.13	-0.01	-0.06	0.02
201889	5600	4.1	-0.85	1.2	0.05	0.23	0.18	0.01	0.34
201891	5850	4.4	-0.96	1	-0.1	0.24	0.04	-0.06	

Table A1: continued.

HD/BD	$T_{\text{eff}}$ , K	$\log g$	[Fe/H]	Vt	[Sr/Fe]LTE	corr <sub>NLTE</sub>	[Sr/Fe]NLTE	[Ba/Fe]NLTE	[Eu/Fe]
204521	5809	4.6	-0.66	1.1	-0.06	0.21	0.05	-0.06	0.3
Hercules stream									
13403	5724	4	-0.31	1.1	-0.06	0.18	0.02	-0.09	0.15
19308	5844	4.3	0.08	1.1	-0.08	0.15	-0.03	-0.01	-0.04
23050	5929	4.4	-0.36	1.1	-0.08	0.18	0.00	-0.04	0.25
30562	5859	4	0.18	1.1	-0.08	0.14	-0.03	0.02	0.02
64606	5250	4.2	-0.91	0.8	0.03	0.24	0.17	-0.14	0.4
68017	5651	4.2	-0.42	1.1	-0.1	0.19	-0.01	-0.12	0.26
81809	5782	4	-0.28	1.3	-0.12	0.18	-0.04	-0.15	0.17
107213	6156	4.1	0.07	1.6	-0.07	0.15	-0.01	0.02	
139323	5204	4.6	0.19	0.7	0.31	0.11	0.32	0.00	0.1
139341	5242	4.6	0.21	0.9	-0.06	0.10	-0.05	-0.07	0.13
144579	5294	4.1	-0.7	1.3	0	0.21	0.11	-0.25	0.24
159222	5834	4.3	0.06	1.2	-0.09	0.15	-0.03	-0.03	-0.07
159909	5749	4.1	0.06	1.1	-0.13	0.14	-0.08	-0.11	-0.03
215704	5418	4.2	0.07	1.1	-0.03	0.13	0.00	-0.12	-0.03
218209	5705	4.5	-0.43	1	-0.08	0.19	0.01	-0.01	-0.03
221354	5242	4.1	-0.06	1.2	-0.12	0.14	-0.07	-0.26	-0.03
nonclassified									
4628	4905	4.6	-0.36	0.5	-0.09	0.16	-0.02	-0.04	
4635	5103	4.4	0.07	0.8	0.03	0.12	0.05	-0.04	0
10145	5673	4.4	-0.01	1.1	-0.11	0.15	-0.05	-0.06	0.15
12051	5458	4.55	0.24	0.5	-0.04	0.11	-0.02	0.1	-0.07
13974	5590	3.8	-0.49	1.1	-0.11	0.19	-0.01	-0.01	0.01
17660	4713	4.75	0.17	1.3	0.03	0.10	0.03	-0.14	0.15
20165	5145	4.4	-0.08	1.1	-0.02	0.14	0.02	-0.07	0
24206	5633	4.5	-0.08	1.1	-0.04	0.15	0.018	0.03	0.07
32147	4945	4.4	0.13	1.1	0.27	0.11	0.28	-0.04	0.06
45067	6058	4	-0.02	1.2	-0.1	0.16	-0.03	0	-0.04
84035	4808	4.8	0.25	0.5	0.11	0.09	0.10	-0.05	-0.08
86728	5725	4.3	0.22	0.9	-0.07	0.13	-0.03	-0.06	-0.1
90875	4788	4.5	0.24	0.5	0.26	0.09	0.25	-0.01	
117176	5611	4	-0.03	1	-0.07	0.15	-0.01	-0.01	0.07
117635	5230	4.3	-0.46	0.7	-0.02	0.18	0.06	-0.04	0.3
154931	5910	4	-0.1	1.1	-0.09	0.16	-0.02	0.01	-0.01
159482	5620	4.1	-0.89	1	-0.03	0.23	0.10	-0.01	0.35
168009	5826	4.1	-0.01	1.1	-0.09	0.15	-0.03	-0.06	0.05
173701	5423	4.4	0.18	1.1	-0.01	0.12	0.01	-0.1	-0.14
182736	5430	3.7	-0.06	1	0.03	0.14	0.07	0.05	
184499	5750	4	-0.64	1.5	-0.04	0.21	0.07	-0.1	0.37
184768	5713	4.2	-0.07	1.1	-0.09	0.15	-0.03	-0.09	0.11
186104	5753	4.2	0.05	1.1	-0.07	0.15	-0.02	-0.05	0.09
215065	5726	4	-0.43	1.1	-0.15	0.19	-0.05	-0.16	
219134	4900	4.2	0.05	0.8	0.05	0.11	0.06	-0.03	-0.11
219396	5733	4	-0.1	1.2	-0.1	0.16	-0.03	-0.09	
224930	5300	4.1	-0.91	0.7	-0.04	0.24	0.10	-0.09	